澳門大學
UNIVERSIDADE DE MACAU
UNIVERSITY OF MACAU

Outstanding Academic Papers by Students
學生優秀作品

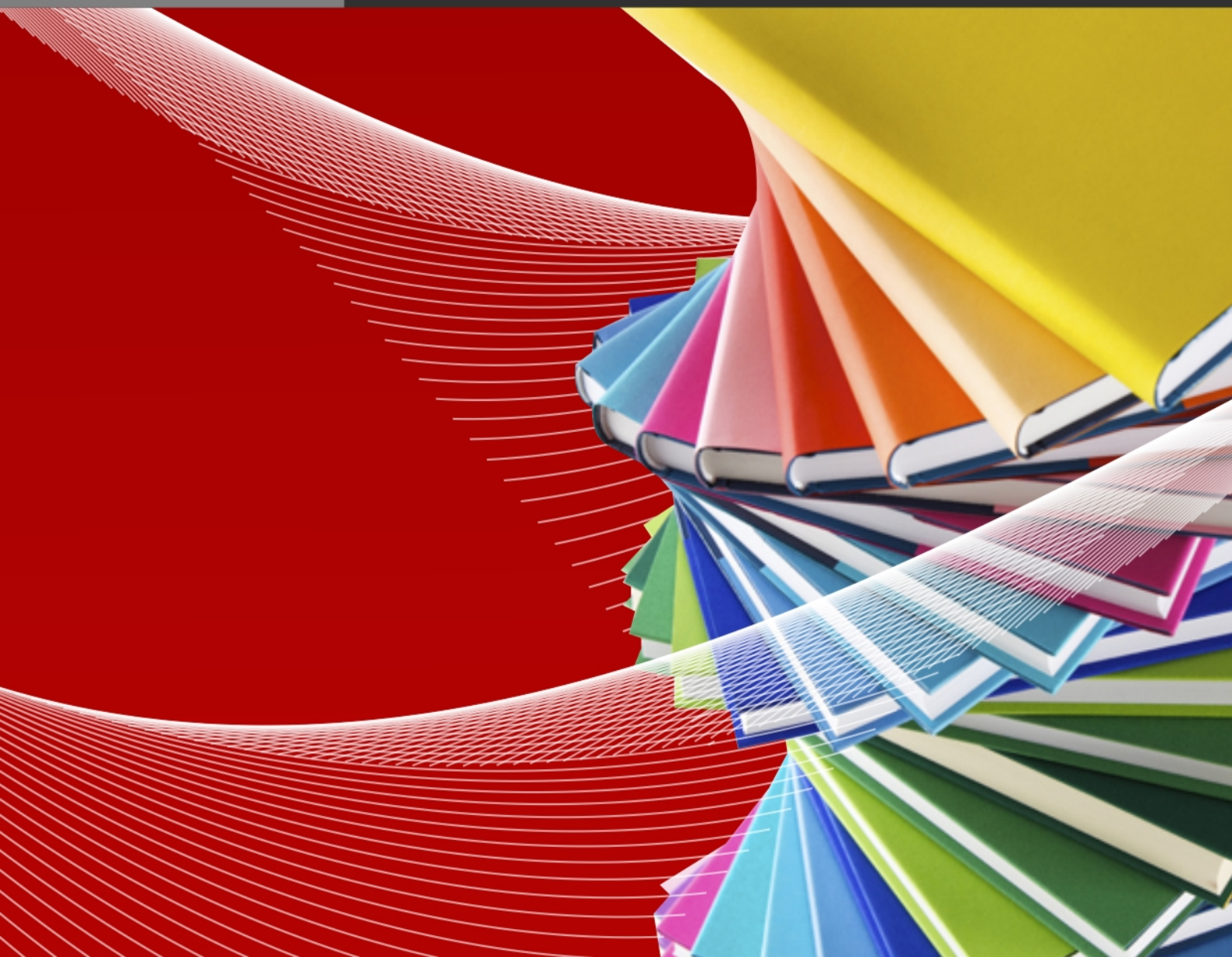

Distortional and Warping Analysis of Rectangular Thin-walled Closed Beams

by

Ng Chi Kin

Final Year Project Report submitted in partial fulfillment
of the requirement of the Degree of

Bachelor of Science in Civil Engineering

2016-2017

Faculty of Science and Technology
University of Macau

UNIVERSIDADE DE MACAU
仁義禮知信
澳門大學

DECLARATION

I declare that the project report here submitted is original except for the source materials explicitly acknowledged and that this report as a whole, or any part of this report has not been previously and concurrently submitted for any other degree or award at the University of Macau or other institutions.

I also acknowledge that I am aware of the Rules on Handling Student Academic Dishonesty and the Regulations of the Student Discipline of the University of Macau.

Signature : NG CHI KIN

Name : NG CHI KIN

Student ID : D-B-32628-6

Date : 16/5/2017

APPROVAL FOR SUBMISSION

This project report entitled "**Distortional and Warping Analysis of Rectangular Thin-walled Closed Beams**" was prepared by Ng Chi Kin in partial fulfillment of the requirements for the degree of Bachelor of Science in Civil Engineering at the University of Macau.

Endorsed by,

Signature : 

Supervisor : Prof. Dr. IU Vai Pan

ACKNOWLEDGEMENTS

The student would like to extend his deepest gratitude to his supervisor, Dr.IU Vai Pan for his full support, valuable comments and infinite patience. The project was completed under his thorough guidance.

There are always challenges on the path to dedication and profession but through these years of study and endless help from every teacher, I myself had developed a very basic sense of how an engineering student should do to deal with the problems and learn from them.

Finally, best wishes to Prof. IU Vai Pan for his good health and happy life.

ABSTRACT

The purpose of this project is to present a warping and distortional analysis of thin-walled box beams. In this project, the behavior of thin-walled box beams in rectangular shape under different loadings and boundary conditions has been studied. The torsional warping and distortion deformations were predicted using pre-assigned functions which formed a stiffness matrix equation to solve the one-dimensional problem using a standard two-node displacement-based C^0-continous finite element approach. A computer program was developed using Fortran Language to carry out the numerical analysis and which was compared with the results using existing Finite Element Method Software – Abaqus shell models. The result was also compared with the work by other researchers to check its accuracy and validity.

Table of Contents

LIST OF FIGURE

LIST OF TABLE

List of symbols

$u_s(s,z)$: Tangential displacement component of each contour

$u_n(s,z)$: Normal displacement component of a point in each contour

$u_z(s,z)$: Longitudinal displacement component of a point in each wall contour

$U(z)$: One-dimensional nodal displacement of torsional warping deformation

$\theta(z)$: One-dimensional nodal displacement of torsional deformation

$\chi(z)$: One-dimensional nodal displacement of distortional deformation

ψ_s^{θ}: Pre-assigned functions of s describing the contour deformation due to torsion

ψ_s^{χ} : Pre-assigned functions describing the contour deformation in the due to distortion

ψ_n^{θ}: Pre-assigned functions of s describing the contour deformation due to torsion

ψ_n^{χ}: Pre-assigned functions of s describing the contour deformation due to distortion

ψ_z^{U}: Pre-assigned functions of s describing the contour deformation due to warping

ψ_{zi}^{U}: Linear hat functions at the ith corner

$\tilde{u}_s(n,s,z)$: Three-Dimensional displacement in the tangential direction of a point in each wall

$\tilde{u}_n(n,s,z)$: Three-Dimensional displacement in the normal direction of a point in each wall

$\tilde{u}_z(n,s,z)$: Three-Dimensional displacement in the normal direction of a point in each wall

ϵ_{zz}: Strain-component in z-axis

ϵ_{zs}: Strain-component in z-s plane

ϵ_{ss}: Strain-component in s-axis

σ_{zz}: Normal stress component in z-axis

σ_{zs}: Stress component in z-s plane

σ_{sz}: Stress component in s-z plane

σ_w: Direct warping stress due to torsion

σ_d: Transverse bending stress due to distortion

E: Young's Modulus

ν: Poisson's ratio

G: Shear Modulus

σ_{xz}: Shear stress component in x-z plane

σ_{yz}: Shear stress component in y-z plane

s_i: Tangential coordinate of a point in i^{th} wall

n: Normal coordinate of a point of each wall towards outward

α_i: Angle in radians between horizontal axis and tangential direction of i^{th} wall

$r(s)$: Distance normal to the contour measured from the Shear Center of the cross-section

l_i: Distance measured from the origin of the s-coordinate on the i^{th} wall to the point N_i

$y(s)$: Y-coordinate which depends on s-coordinate of a point

$x(s)$: X-coordinate which depends on s-coordinate of a point

A_1: Area enclosed by the contours

$\beta_{i(i)}$: Rotations of the ith wall at the ith corner

$\beta_{i(i+1)}$: Rotations of the ith wall at the (i+1)th corner

b_i: Length of the ith wall

t: Uniform contour thickness assumed to be much smaller than the beam length

$\bar{M}_{i(i)}$: Transverse bending moment of ith wall at (i)th corner

$\bar{M}_{i(i+1)}$: Transverse bending moment of ith wall at (i+1)th corner

p_1: One-dimensional external load term in the axial direction due to warping

q_1: One-dimensional external load term in the tangential direction due to torsion

q_2: One-dimensional external load term in the tangential direction due to warping

H: Generalized Torsional Stress resultants

B: Generalized Warping Stress resultants

Q: Generalized Distortional Stress resultants

γ_t: Twisting angle of the cross-section in radians

γ_d: Distortion angle of the cross-section in radians

ψ_z: Angle of rotation of the flange in radians

ϕ_z: Angle of rotation of the web in radians

Chapter 1 Introduction

Thin-walled box beams are currently widely used in bridges due to the high torsional rigidities and space-saving properties with overhead bridges. Various types of box beams such as straight box girders, curved box girders, box girders with cantilever slabs and pre-stressed concrete beams are used for light rails deck, bridges. However, the deformation behavior of the cross-section is rather complex, which it is very difficult to accurately predict their behaviors with elementary beam theory.

In this project, the static coupled deformations as torsion, warping and distortion of thin-walled closed beams with rectangular cross-sections were analyzed using one-dimensional beam theory proposed. A two-node C^0 finite element computer program was developed for numerical analysis. Finite Element Models using Abaqus software were also used to verify the numerical solution of the proposed theory.

1.1 Background

Rectangular beams have been the most popular structural elements in most of the modern superstructure. Nowadays, thin-walled beams or girders are widely used in bridges or overhead structures due to its torsional rigidity and cost-saving properties. Thin-walled beams refer to beams with the thickness of the wall (contour) is significantly thinner than the length (width) of the wall (contour), the top flange of thin-walled beams are also under various type of loading and diaphragms can be used to strengthen the rigidity of the cross-section especially in long-span structure. The usual design approach for rectangular beams was using the elementary beam theory, in which the cross-section of the beams do not deform, resulting only in longitudinal bending and every cross-section of the beam remains plane.

The self-weight of bridge structures is a major concern for the engineers as the self-weight of the structure dominates the loading compared to live loads. Therefore, an effective and efficient design always aim on decreasing the self-weight while assuring the rigidity as well as the overall stability, especially for long-span bridges. The Sutong Bridge in China shown in Fig.1.1 was constructed using precast segmental method with single-cell box girder, consists of 30m, 50m and 70m span. The Matagorda Segmental Bridge shown in Fig1.2. is also a pre-cast segmental bridge structure with deck width of 14m, while spanning in 54 and 108m.

Typical thin-walled beams are usually in rectangular or trapezoidal shapes. The elementary beam theory would not be used in designing thin-walled structures as the cross-section deformation cannot be neglected, which is significant to the structural element, when subjected to unsymmetrical loading. Major considerations of deformation of thin-

walled beams are, most of the case, shear-lag effect (for girders), distortion and warping deformation. In this project, the coupled deformation of distortion and torsional warping of the cross-section of rectangular beams under torsional-equivalent loadings were analyzed.

Fig. 1.1 - Sutong Precast Segmental Bridge, China

Fig. 1.2 - Matagorda Precast Segmental Bridge, Texas

1.2 Introduction to Warping and Distortion Deformation

The usual structural behavior under eccentric loading of box beams (girders) is illustrated as Fig.1.2.1. A line load or concentrated load acting on the tip of the cross-section results in bending, torsion and distortion stress. The bending deflection can be approximated using the elementary beam theory if the shear lag effect is not significant, however, the torsional and distortional deformation cannot be accurately calculated using the classical beam theory as the cross-section no longer remains plane.

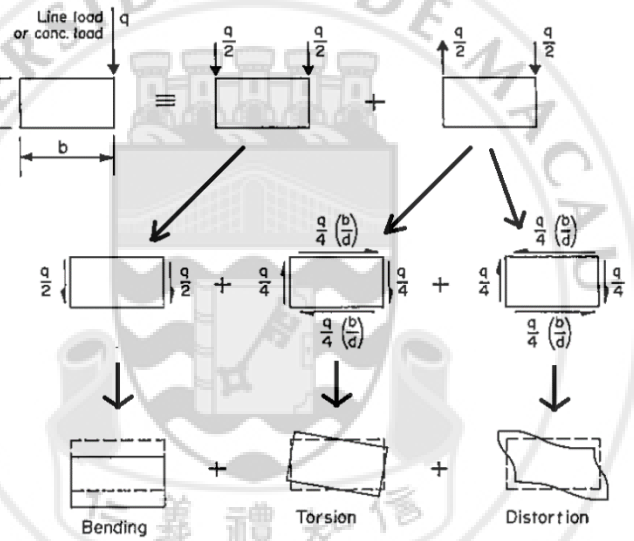

Fig. 1.2.1 - Decomposing an eccentric loading

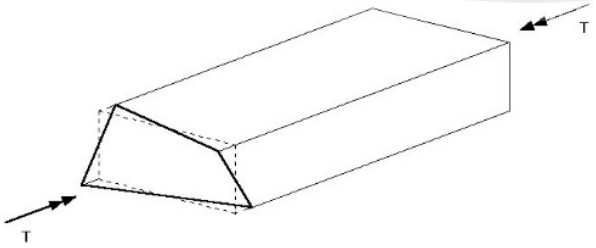

Fig. 1.2.2 - Torsion Warping Deformation

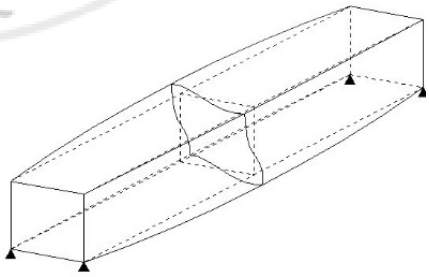

Fig. 1.2.3 - Distortion Deformation

The warping deformation being studied in this project is only due to torsion, the distortional warping is not considered. As shown in Fig.1.2.2, the four corners deform axially in compression and tension, resulting a non-planar cross-section. Many researches had been made on the warping function to predict the warping deformation which is a linear function of the dimensions of the cross-section. The warping behavior is more significant for thin-walled open sections as H or I shape beams. Examples of warping function of a cross-section are shown in Fig.1.2.4, the warping function in 1.2.4(c) has a balanced effect of four corners and zero value at the middle of each contour, resulting maximum value at each corner and the function varies linearly along the contour. In this report, only the warping deformation of the corners are discussed as it is the most critical in the cross-section.

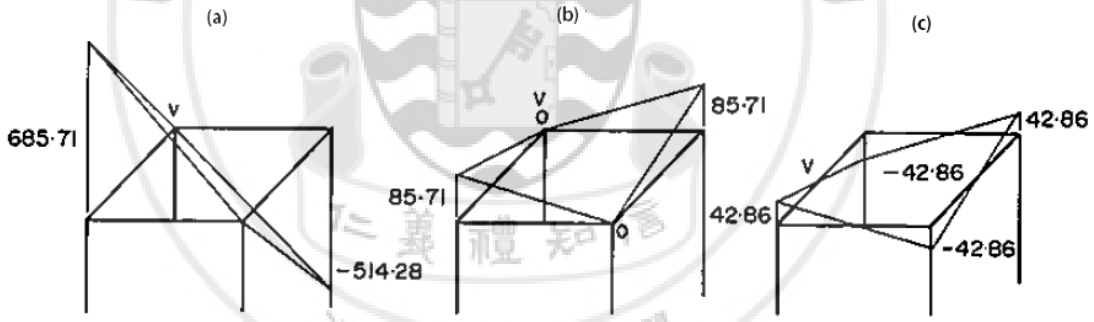

Fig. 1.2.4 - Warping function of a rectangular cross-section

The distortion function, however, is more complex as it is not linear function along the contour. Kim & Kim (1999) proposed a cubic distortion function to predict the deformation of each contour which will be verified in the report.

1.3 Objectives and Scope

Based on the limited research work on the torsional warping and distortion behavior of thin-walled box beams mentioned in the introduction, the objectives and scopes which were established for this report as following:

- To study the deformation behavior of thin-walled box beams under torsional loading
- To understand the pre-assigned deformation functions and constants governing the deformation behavior of thin-walled box beams
- To understand the derivation of the governing equations based on the principle of minimum potential energy
- To develop a one-dimensional finite-element computer program to solve the problem of thin-walled box beams
- To validate the developed computer program and verify the solution to the research works by previous researchers
- To establish valid finite element models of thin-walled box beams using existing ABAQUS Finite Element Software and verify the proposed method
- To compare the numerical solution with the finite element model analysis and discuss the differences

Chapter 2 Literature Review

In 1961, Vlasov (1961) offered a comprehensive theoretical analysis of thin-walled structures. Vlasov (1961) showed that the distortional effects could be described using a fourth order ODE in a displacement quantity, referred as Beam on Elastic Foundation. The analogy was then further developed by Wright et.al. to predict the warping and distortional stresses. In the analogy, the beam behavior results from in-plane bending of the box beam walls, while the elastic foundation effect is provided by the beam's transverse bending stiffness which is the resistance to distortion.

In 1983, Boswell and Zhang(1983) presented a finite beam element formulation for the static analysis and later reported related experimental results in 1985. The static analysis included warping, distortion and shear-lag effect of straight and curved thin-walled box beams with varying cross-section. In the experiment, three steel models consisting straight single-cell cantilever, curved sing-cell cantilever and a simply-supported twin box had been constructed. The distortional angle and twisting angle of the cross-section were evaluated from the observed values of displacements. The additional stress system arising from the torsional warping and distortion effects were also calculated by a one-dimensional finite element analysis using thin-walled box beam elements and the results were in close agreement.

The straight single-cell cantilever problem was then analyzed by Balch and Steele in 1987, by a perturbation procedure. Equations of conventional thin plate theory were used to formulate an eigenvalue problem for effects of self-equilibrating end loads. In the asymptotic solutions by Balch and Steele assumptions were made that the in-plane shear strain was negligible and the stress distribution varies linearly along the contour.

However, the analysis was only restricted to closed rectangular cross sections with uniform thickness.

Based on the theories mentioned above, Kim & Kim(1999) further proposed a cubic distortion function and the continuity condition of rotation of corners which can be applied to general quadrilateral cross sections. Pre-assigned functions were used to describe the section deformations using one-dimensional theory to analyze static and free-vibration problems which the results were compared with the existing finite plate finite element solution. In this project, the work was mainly based on the method proposed by Kim & Kim(1999) and the results were compared with existing Finite Element Method computer program Abaqus models.

Chapter 3 Methodology

In this project, the work was based on the theory proposed by Kim & Kim (1999), who imposed the continuity condition of the rotation/moment of corners with a cubic distortion function. By selecting the appropriate pre-assigned functions describing the contour deformations as twisting, warping and distortion, a one-dimensional Finite Element analysis was performed using Fortran95 language. The numerical results were then compared to the work by Boswell & Zhang (1985) , Balch and Steele (1987), and the existing Finite Element Method computer program ABAQUS.

3.1Basic Field Equations and Assumptions

Assumptions:

- Uniform contour thickness t is assumed to be much smaller than the length of the beam; Width of flange is denoted as b; Height of web is denoted as h
- The contour (wall) is assumed to be in-extensional, i.e.($\frac{\partial u_s}{\partial s} = 0$) , the tangential displacement is uniform across the contour length
- A right - handed curvilinear coordinate system(n,s,z) was used in addition to the Cartesian Coordinate(x,y,z) in Fig.1
- The tangential coordinate s is measured along the contour, origin of s varies from each wall, rotate in anti-clockwise direction
- The normal coordinate n is measured from the middle line of each contour directs outwards from the contour for positive value
- The transverse shear effect of the cross-section is neglected

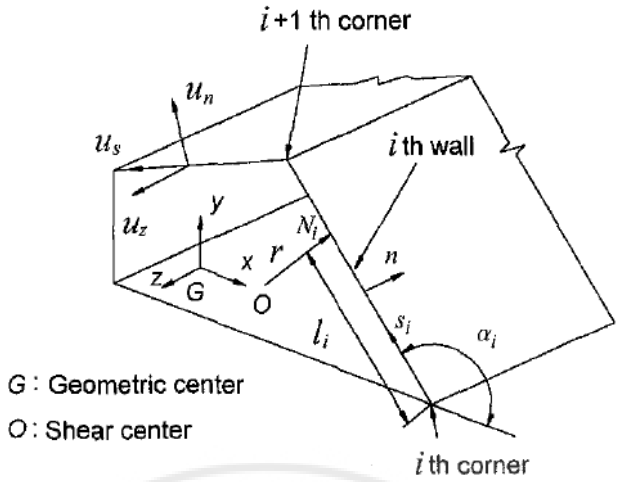

Fig. 3.1 - Displacements of an arbitrary point on the contour of the thin-walled cross section

Field equations:

In this project, only the measures of torsion, warping and distortion were considered as field variables. The three-dimensional displacements ($\tilde{u}_s, \tilde{u}_n, \tilde{u}_z$) of a point on the cross-section were expressed as shell displacements (u_s, u_n, u_z) of a point on the contour (Fig.3.1):

- normal $u_n(s,z)$, which directs outward from the contour
- tangential $u_s(s,z)$, in the direction of anti-clockwise rotation of each contour
- axial $u_z(s,z)$, positive in the z-axis

$$u_s(s,z) = \psi_s^{\theta}(s) \cdot \theta(z) + \psi_s^{U}(s) \cdot U(z) + \psi_s^{\chi}(s) \cdot \chi(z) \qquad (1a)$$

$$u_n(s,z) = \psi_n^{\theta}(s) \cdot \theta(z) + \psi_n^{U}(s) \cdot U(z) + \psi_n^{\chi}(s) \cdot \chi(z) \qquad (1b)$$

$$u_z(s,z) = \psi_z^{\theta}(s) \cdot \theta(z) + \psi_z^{U}(s) \cdot U(z) + \psi_z^{\chi}(s) \cdot \chi(z) \qquad (1c)$$

The $\psi(s)$ in Eq.(1) denote the preassigned functions of s describing the contour deformations in the n-s plane per unit value of U, θ and χ due to warping, torsion and distortion respectively. The major issue was to find the correct form of $\psi(s)$, particular for the distortion function $\psi^{\chi}(s)$.

Torsional deformation (Twisting)

To consider the torsional deformation (twisting) $\theta(z)$ of the cross-section about the positive z-axis, the axial deformation (ψ_z^{θ}) can be considered as 0, one can identify as :

$$\psi_s^{\theta}(s) = r(s)$$

$$\psi_n^{\theta}(s) = -\ell_i + s$$

$$\psi_z^{\theta}(s) = 0 \qquad (2)$$

*Where r(s) is the distance normal to the contour from the shear center O,

*And ℓ_i is the distance from the origin of the s coordinate on the i^{th} wall to the point N_i

Torsional warping deformation

To consider warping deformation $U(z)$ of the cross-section, only axial displacement $u_z(s,z)$ is significant, one can identify as :

$$\psi_s^{U}(s) = 0$$

$$\psi_n^{U}(s) = 0$$

$$\psi_z^{U}(s) \neq 0 \qquad (3)$$

Distortional deformation

To consider the in-plane distortional deformation $\chi(z)$ of the cross-section, the axial displacement is considered to be zero, one then can also identify as:

$$\psi_s^{\chi}(s) \neq 0$$

$$\psi_n^{\chi}(s) \neq 0$$

$$\psi_z^{\chi}(s) = 0 \qquad (4)$$

Three-dimensional displacements: $\tilde{u}_n$, $\tilde{u}_s$ and $\tilde{u}_z$ of any point in a wall can then be calculated with uniform wall thickness t, thus

$$\tilde{u}_n(n,s,z) \approx u_n(s,z) = \psi_n^{\theta}(s)\cdot\theta(z) + \psi_n^{\chi}(s)\cdot\chi(z) \qquad (5a)$$

$$\tilde{u}_s(n,s,z) \approx u_s(s,z) + n\frac{\partial u_n(s,z)}{\partial s}$$

$$= \psi_s^{\theta}(s)\cdot\theta(z) + \psi_s^{\chi}(s)\cdot\chi(z) + \frac{\partial\psi_n^{\chi}(s)}{\partial s}\cdot\chi(z) \qquad (5b)$$

$$\tilde{u}_z(n,s,z) \approx u_z(s,z) = \psi_z^{U}(s)\cdot U(z) \qquad (5c)$$

Eq.(5) are then used to calculate the three-dimensional strain components:

$$\epsilon_{zz} = \frac{\partial\tilde{u}_z}{\partial z} = \psi_z^{U}(s)\cdot\frac{d\,U(z)}{dz} \qquad (6a)$$

$$\epsilon_{zs} = \frac{1}{2}\left(\frac{\partial\tilde{u}_z}{\partial s} + \frac{\partial\tilde{u}_s}{\partial z}\right)$$

$$\approx \frac{1}{2}\left(\frac{d\,\psi_z^{U}(s)}{ds}\cdot U(z) + \psi_s^{\theta}(s)\cdot\frac{d\,\theta(z)}{dz} + \psi_s^{\chi}(s)\cdot\frac{d\,\chi(z)}{dz}\right) \qquad (6b)$$

$$\epsilon_{ss} = \frac{\partial\tilde{u}_s}{\partial s} = n\frac{\partial^2 u_n}{\partial s^2} = n\frac{\partial^2\psi_n^{\chi}(s)}{\partial s^2}\cdot\chi(z) \qquad (6c)$$

Note: Eq.(6c) is obtained with the assumption $\frac{\partial u_s}{\partial s} = 0$

Other Strains components are negligible compared to those components.

Three-dimensional Stress components:

$$\sigma_{zz} = E_1 (\epsilon_{zz} + \upsilon\epsilon_{ss})$$

$$\sigma_{ss} = E_1 (\epsilon_{ss} + \upsilon\epsilon_{zz})$$

$$\sigma_{zs} = 2G\epsilon_{zs} \quad (7)$$

Where $E_1 \equiv \frac{E}{1-\upsilon^2}$ and E, G are Young's and Shear Moduli, respectively; υ is the Poisson's ratio

3.2 Warping and Distortion Functions

The warping (ψ_z^U) and distortion functions ($\psi_{si}^\chi, \psi_{ni}^\chi$) were approximated by imposing the condition that the virtual work done by warping and distortion stresses vanish under rigid-body virtual displacement fields.

Virtual translations and rotations are denoted as :

- $\delta U_x\ , \delta U_y, \delta U_z -$ Virtual translation in x, y and z directions, respectively
- $\delta\Theta_x, \delta\Theta_y, \delta\Theta_z -$ Virtual Rotation in x, y and z directions, respectively

Warping Function ψ_z^U:

Non-zero stress components by warping given by strains in Eq. (6) and Eq. (7):

$$\sigma_{zz}^U(z) = E_1 \cdot \psi_z^U(s) \frac{d\,U(z)}{dz} \quad , \quad \sigma_{sz}^U(z) = G \cdot \frac{d\,\psi_z^U}{ds} \cdot U(z) \tag{9}$$

When warping deformation is being considered, it is generally resulting from flexural and torsional deformations, which means that the virtual work done due to $\delta \mathrm{U}_x, \delta \mathrm{U}_y \; and \; \delta\Theta_z$ does not generally vanish, then there will be no condition to find the function ψ_z^U from Eq.(10) under this consideration.

$$\delta W_{warping} = \int_A \left[r(s) \cdot \quad \sigma_{sz}^U(z)\delta\Theta_z - \quad \sigma_{sz}^U(z) \cdot \delta \mathrm{U}_x + \quad \sigma_{sz}^U(z) \cdot \delta \mathrm{U}_y \right] dA \quad \neq 0 \tag{10}$$

However, no virtual work should be done by the warping stress due to the rigid-body motions associated with axial extension (δU_z) and bending motions $\left(y(s) \cdot \delta\Theta_x, \; x(s) \cdot \delta\Theta_y\right)$:

$$\delta W_{warping} = \int_A \sigma_{zz}^U(z) \left[\delta U_z - y(s) \cdot \delta\Theta_x + x(s) \cdot \delta\Theta_y \right] dA \; = 0 \tag{11}$$

Each of the terms in Eq.(11) should be zero in any case:

$$\int_A \psi_z^U \, dA = 0 \tag{12a}$$

$$\int_A y(s) \cdot \psi_z^U \, dA = 0 \tag{12b}$$

$$\int_A x(s) \cdot \psi_z^U \, dA = 0 \tag{12c}$$

The warping function using the Saint Venant Torsion theory that the shear strain due to warping is negligible compared to the Saint Venant shear strain.

The warping function is chosen as :

$$\psi_z^U(s) = \int_0^s (r - r_n) dA \tag{13}$$

Which

$$r_n = 2A_1 / \oint ds \tag{14}$$

,where A_1 and $\oint ds$ are the area enclosed by and the total length of the contour respectively.

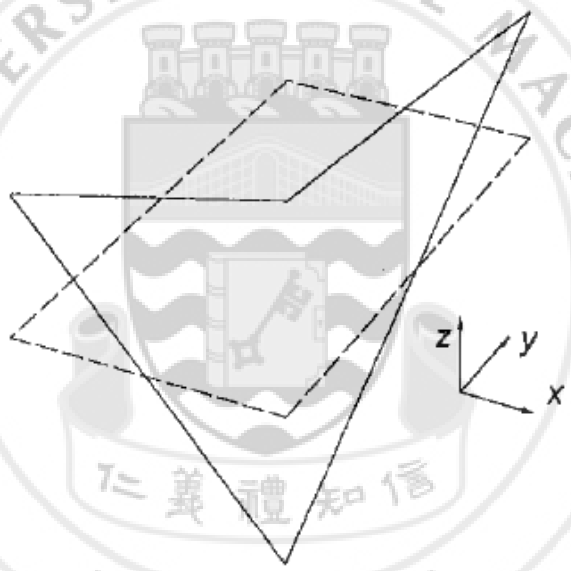

Fig. 3.2.1 - Warping function of a rectangular cross-section

The warping function of the cross-section is then plotted as shown in Fig.3.2.1 which is a linear function depends on the s-coordinate, the middle point of each wall has a zero value and maximum value at the corners.

Distortion function $\psi_{si}^{\chi}, \psi_{ni}^{\chi}$

The distortion functions $\psi_{si}^{\chi}, \psi_{ni}^{\chi}$ proposed by Kim & Kim (1999) is presented in this section and validated in the subsequent section. In the assumption, each wall is in-extensional, i.e.($\frac{\partial u_s}{\partial s} = 0$), therefore rigid body deformation of each wall in the plane of the cross-section is also assumed.

Cross-section displacements are denoted as :

- $\bar{\psi}_{si}^{\chi}(s_i),\ \bar{\psi}_{ni}^{\chi}(s_i)$ – Tangential and normal translations of the i[th] wall measured at the center of each wall
- $\bar{\psi}_{\theta_i}^{\chi}$ – Rigid-body rotation of the i[th] wall measured at the center of each wall
- $i = 1,2,3,4\ ;\ 5 \rightarrow 1$

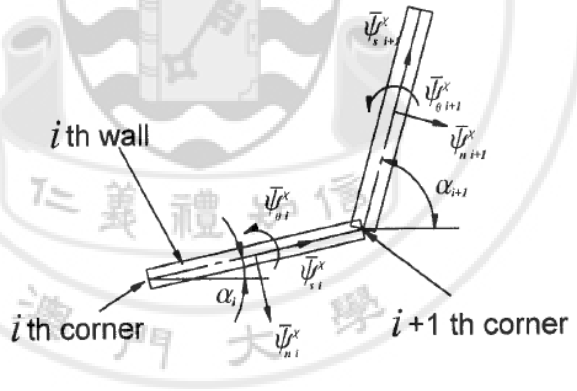

Fig. 3.2 - Variables defining the in-plane deformation of the i[th] wall, associated with the contour distortion

$$\psi_{si}^{\chi}(s_i) = \bar{\psi}_{si}^{\chi} \qquad (15a)$$

$$\psi_{ni}^{\chi}(s_i) = \bar{\psi}_{ni}^{\chi} - \left(s_i - \frac{b_i}{2}\right) \bar{\psi}_{\theta i}^{\chi}\ ,\ (0 \le s_i \le b_i, i = 1,2,3,4) \qquad (15b)$$

where b_i denotes the length of the wall

Displacement Continuity conditions:

$$\psi_{s_i}^{\chi}|_{s_i=b_i} = \psi_{s_{i+1}}^{\chi}|_{s_{i+1}=0} \cdot \cos(\alpha_{i+1} - \alpha_i) - \psi_{n_{i+1}}^{\chi}|_{s_{i+1}=0} \cdot sin(\alpha_{i+1} - \alpha_i) \qquad (16a)$$

$$\psi_{n_i}^{\chi}|_{s_i=b_i} = \psi_{s_{i+1}}^{\chi}|_{s_{i+1}=0} \cdot \sin(\alpha_{i+1} - \alpha_i) + \psi_{n_{i+1}}^{\chi}|_{s_{i+1}=0} \cdot cos(\alpha_{i+1} - \alpha_i) \qquad (16b)$$

$$(for\ i = 1,2,3,4\ ;5 \rightarrow 1)$$

By applying the Virtual work principle, virtual work by the distortion stress σ_{sz}^{χ} due to the rigid-body virtual displacements $\delta \mathrm{U}_x, \delta \mathrm{U}_y\ and\ \delta\Theta_z$ corresponding to flexural and torsional deformations must vanish:

$$\delta W_{distortion} = 0 = \int_A \left[r(s) \cdot \sigma_{sz}^{\chi} \cdot \delta\Theta_z + \sigma_{zx}^{\chi} \cdot \delta \mathrm{U}_x + \sigma_{zy}^{\chi} \cdot \delta \mathrm{U}_y \right] dA \qquad (17)$$

Each of the terms must be zero in any cases:

$$\sum_{i=1}^{4} \int r(s_i) \cdot \left(\sigma_{sz}^{\chi}\right)_i dA = 0 \qquad (18a)$$

$$\sum_{i=1}^{4} \int \left(\sigma_{sz}^{\chi}\right)_i \cdot cos\ \alpha_i\ dA = 0 \qquad (18b)$$

$$\sum_{i=1}^{4} \int \left(\sigma_{sz}^{\chi}\right)_i \cdot sin\ \alpha_i\ dA = 0 \qquad (18c)$$

Normal Displacement $\psi_{ni}^{\chi}(s_i)$ in Eq.(15b) is replaced by a cubic function, the quantities of $\beta_{i(i)}$ and $\beta_{i(i+1)}$ representing the rotations of the ith wall at the ith and (i+1)th corners are introduced to satisfy the rotation/moment continuity condition.

$$\psi_{ni}^{\chi}(s_i) = D_{i0} + D_{i1} \cdot s_i + D_{i2} \cdot {s_i}^2 + D_{i3} \cdot {s_i}^3 \qquad (19)$$

To satisfy the conditions 20a-20d:

$$\psi_{n_i}^{\chi}|_{s_i=0} = \bar{\psi}_{n_i}^{\chi} + \bar{\psi}_{\theta_i}^{\chi} \cdot \frac{b_i}{2} \qquad (20a)$$

$$\psi_{n_i}^{\chi}|_{s_i=b_i} = \bar{\psi}_{n_i}^{\chi} - \bar{\psi}_{\theta_i}^{\chi} \cdot \frac{b_i}{2} \qquad (20b)$$

$$\frac{d}{ds_i}\left[\psi_{n_i}^{\chi}(s_i)\right]_{s_i=0} = \beta_{i(i)} \qquad (20c)$$

$$\frac{d}{ds_i}\left[\psi_{n_i}^{\chi}(s_i)\right]_{s_i=b_i} = \beta_{i(i+1)} \qquad (20d)$$

From (20a), $\psi_{n_i}^{\chi}|_{s_i=0} = D_{i0} = \bar{\psi}_{n_i}^{\chi} + \bar{\psi}_{\theta_i}^{\chi} \cdot \frac{b_i}{2}$

$$\therefore D_{i0} = \bar{\psi}_{n_i}^{\chi} + \bar{\psi}_{\theta_i}^{\chi} \cdot \frac{b_i}{2} \qquad (20\text{-}1)$$

From (20c),

$$\beta_{i(i)} = \frac{d}{ds_i}\left[\psi_{n_i}^{\chi}(s_i)\right]_{s_i=0} = \frac{d}{ds_i}\left[\bar{\psi}_{n_i}^{\chi} + \bar{\psi}_{\theta_i}^{\chi} \cdot \frac{b_i}{2}\right]_{s_i=0}$$

$$= D_{i1} + 2\,D_{i2} \cdot s_i + 3\,D_{i3} \cdot {s_i}^2 + \frac{d\left(\bar{\psi}_{\theta_i}^{\chi}\right)}{ds_i} \cdot \frac{b_i}{2}$$

$$\therefore \; D_{i1} = \beta_{i(i)} \qquad (20\text{-}2)$$

From (20d)

$$\frac{d}{ds_i}\left[\psi_{n_i}^{\chi}(s_i)\right]_{s_i=b_i} = D_{i1} + 2\,D_{i2} \cdot b_i + 3\,D_{i3} \cdot {b_i}^2 + \frac{d\left(\bar{\psi}_{\theta_i}^{\chi}\right)}{ds_i} \cdot \frac{b_i}{2} = \beta_{i(i+1)}$$

$$D_{i2} = \frac{\beta_{i(i+1)} - D_{i1} - 3\,D_{i3} \cdot {b_i}^2}{2b_i} = \frac{\beta_{i(i+1)} - \beta_{i(i)} - 3\,D_{i3} \cdot {b_i}^2}{2b_i} \qquad (20\text{-}3)$$

From (20a-d)

$$\bar{\psi}_{n_i}^{\chi} = \psi_{n_i}^{\chi}|_{s_i=0} - \bar{\psi}_{\theta_i}^{\chi} \cdot \frac{b_i}{2} = \psi_{n_i}^{\chi}|_{s_i=b_i} + \bar{\psi}_{\theta_i}^{\chi} \cdot \frac{b_i}{2}$$

Where $\psi_{n_i}^{\chi}|_{s_i=0} = D_{i0}$,

And $\psi_{n_i}^{\chi}|_{s_i=b_i} = D_{i0} + D_{i1} \cdot b_i + D_{i2} \cdot {b_i}^2 + D_{i3} \cdot {b_i}^3$

Then $D_{i0} - \bar{\psi}_{\theta_i}^{\chi} \cdot \frac{b_i}{2} = D_{i0} + D_{i1} \cdot b_i + D_{i2} \cdot {b_i}^2 + D_{i3} \cdot {b_i}^3 + \bar{\psi}_{\theta_i}^{\chi} \cdot \frac{b_i}{2}$

$$D_{i1} \cdot b_i + D_{i2} \cdot {b_i}^2 + D_{i3} \cdot {b_i}^3 + \bar{\psi}_{\theta_i}^{\chi} \cdot b_i = 0$$

Substitute Eq.(20-1,20-2,20-3) into the above equation

Becomes $\beta_{i(i)} \cdot b_i + \frac{\beta_{i(i+1)} - \beta_{i(i)} - 3\, D_{i3} \cdot {b_i}^2}{2b_i} \cdot {b_i}^2 + D_{i3} \cdot {b_i}^3 + \bar{\psi}_{\theta_i}^{\chi} \cdot b_i = 0$

$$\beta_{i(i)} + \frac{\beta_{i(i+1)} - \beta_{i(i)} - 3\, D_{i3} \cdot {b_i}^2}{2} + D_{i3} \cdot {b_i}^2 + \bar{\psi}_{\theta_i}^{\chi} = 0$$

$$-\frac{1}{2} D_{i3} \cdot \left({b_i}^2\right) + \frac{\beta_{i(i+1)} + \beta_{i(i)} + 2\bar{\psi}_{\theta_i}^{\chi}}{2} = 0$$

$$D_{i3} = \frac{\beta_{i(i+1)} + \beta_{i(i)} + 2\bar{\psi}_{\theta_i}^{\chi}}{{b_i}^2}$$

(20-4)

(20-3) now becomes :

$$D_{i2} = \frac{\beta_{i(i+1)} - \beta_{i(i)} - 3\, D_{i3} \cdot {b_i}^2}{2b_i} = \frac{\beta_{i(i+1)} - \beta_{i(i)} - 3\dfrac{\beta_{i(i+1)} + \beta_{i(i)} + 2\bar{\psi}_{\theta_i}^{\chi}}{{b_i}^2} \cdot {b_i}^2}{2b_i}$$

$$D_{i2} = \frac{\beta_{i(i+1)} - \beta_{i(i)} - 3 \cdot (\beta_{i(i+1)} + \beta_{i(i)} + 2\bar{\psi}_{\theta_i}^{\chi})}{2b_i}$$

$$D_{i2} = \frac{\beta_{i(i+1)} - \beta_{i(i)} \ -3\beta_{i(i+1)} - 3\beta_{i(i)} - 6\bar{\psi}^{\chi}_{\theta_i})}{2b_i}$$

$$D_{i2} = -\frac{\beta_{i(i+1)} + 2\beta_{i(i)} + 3\bar{\psi}^{\chi}_{\theta_i}}{b_i}$$

Then Eq(19) can be written as:

$$\psi^{\chi}_{ni}(s_i) = \bar{\psi}^{\chi}_{n_i} + \bar{\psi}^{\chi}_{\theta_i} \cdot \frac{b_i}{2} + \beta_{i(i)} \cdot s_i - \frac{\beta_{i(i+1)} + 2\beta_{i(i)} + 3\bar{\psi}^{\chi}_{\theta_i}}{b_i} \cdot {s_i}^2 + \frac{\beta_{i(i+1)} + \beta_{i(i)} + 2\bar{\psi}^{\chi}_{\theta_i}}{{b_i}^2} \cdot {s_i}^3 \quad (21)$$

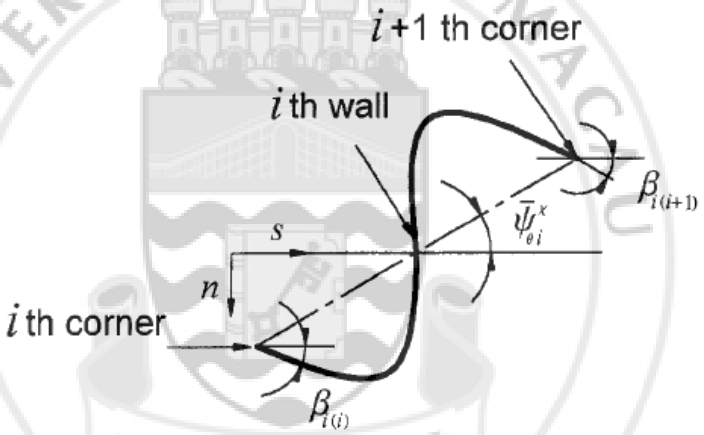

Fig. 3.3 - Typical deformed shape of the i[th] wall of a thin-walled beam

In order to find the eight coefficients $\beta_{i(i)}, \beta_{i(i+1)}$ where i =1,2,3,4 , Rotation and Moment continuity at i^{th} and $i+1^{th}$ corners at i^{th}wall must be satisfied :

$$\beta_{i(i+1)} = \beta_{i+1(i+1)} \quad (22a)$$

$$\bar{M}_{i(i+1)} = \bar{M}_{i+1(i+1)} (22b)$$

The moments $\bar{M}_{i(i)}$and $\bar{M}_{i(i+1)}$ of the i^{th} wall at the i^{th} and $i+1^{th}$ corners are given by:

$$\bar{M}_{i(i)} = M_i(s_i = 0), \ \bar{M}_{i(i+1)} = M_i(s_i = b_i)$$

The moment $\bar{M}_i\,(s_i)$ of the i^{th} wall can be approximated by classical beam theory $M = EIy''$

$$\bar{M}_i\,(s_i) = \frac{Et^3}{12} \cdot \frac{d^2\,\psi_{n_i}^{\chi}}{ds_i{}^2}$$, where t = thickness of the wall

Deriving Distortional constants

Solving for 12 constants for distortion function ($\bar{\psi}_{si}^{\chi}, \bar{\psi}_{n_i}^{\chi}, \bar{\psi}_{\theta_i}^{\chi}$, i = 1,2,3,4):

For these 12 constants, there are 11 conditions that can solve 11 unknowns where one of the twelve can be set arbitrary. In this paper, $\bar{\psi}_{s1}^{\chi}$ is assumed to be known value, 11 equations are therefore written in terms of $\bar{\psi}_{s1}^{\chi}$.

Solving for the tangential translation constants $\bar{\psi}_{si}^{\chi}$, Eq(18) must be satisified.

$$\sum_{i=1}^{4} \int r(s_i) \cdot \left(\sigma_{sz}^{\chi}\right)_i dA = 0 \qquad (18a)$$

$$\sum_{i=1}^{4} \int \left(\sigma_{sz}^{\chi}\right)_i \cdot cos\ \alpha_i\ dA = 0 \qquad (18b)$$

$$\sum_{i=1}^{4} \int \left(\sigma_{sz}^{\chi}\right)_i \cdot sin\ \alpha_i\ dA = 0 \qquad (18c)$$

The virtual work by the distortion stress $\sigma_{sz}^{\chi}(s)$ must be zero, Eq(18) then becomes

$$\sum_{i=1}^{4} \int r(s_i) \cdot \left(\sigma_{sz}^{\chi}\right)_i dA = \sum_{i=1}^{4} r(s_i) \cdot \bar{\psi}_{si}^{\chi} \cdot b_i \cdot t = 0 \quad (18a)$$

$$\sum_{i=1}^{4} \int \left(\sigma_{sz}^{\chi}\right)_i \cdot cos\ \alpha_i\ dA = \sum_{i=1}^{4} cos\ \alpha_i \cdot \bar{\psi}_{si}^{\chi} \cdot b_i \cdot t = 0 \quad (18b)$$

$$\sum_{i=1}^{4} \int \left(\sigma_{sz}^{\chi}\right)_i \cdot sin\ \alpha_i\ dA = \sum_{i=1}^{4} sin\ \alpha_i \cdot \bar{\psi}_{si}^{\chi} \cdot b_i \cdot t = 0 \quad (18c)$$

Thus:

$$r_1 \cdot \bar{\psi}_{s1}^{\chi} \cdot b_1 \cdot t + r_2 \cdot \bar{\psi}_{s2}^{\chi} \cdot b_2 \cdot t + r_3 \cdot \bar{\psi}_{s3}^{\chi} \cdot b_3 \cdot t + r_4 \cdot \bar{\psi}_{s4}^{\chi} \cdot b_4 \cdot t = 0 \quad (18a')$$

$$\cos\alpha_1 \cdot \bar{\psi}_{s1}^{\chi} \cdot b_1 \cdot t + \cos\alpha_2 \cdot \bar{\psi}_{s2}^{\chi} \cdot b_2 \cdot t + \cos\alpha_3 \cdot \bar{\psi}_{s3}^{\chi} \cdot b_3 \cdot t + \cos\alpha_4 \cdot \bar{\psi}_{s4}^{\chi} \cdot b_4 \cdot t = 0 \quad (18b')$$

$$\sin\alpha_1 \cdot \bar{\psi}_{s1}^{\chi} \cdot b_1 \cdot t + \sin\alpha_2 \cdot \bar{\psi}_{s2}^{\chi} \cdot b_2 \cdot t + \sin\alpha_3 \cdot \bar{\psi}_{s3}^{\chi} \cdot b_3 \cdot t + \sin\alpha_4 \cdot \bar{\psi}_{s4}^{\chi} \cdot b_4 \cdot t = 0 \quad (18c')$$

From Eq(18a),

$$\bar{\psi}_{s2}^{\chi} = \frac{1}{r_2 \cdot b_2} \cdot [-r_3 \cdot \bar{\psi}_{s3}^{\chi} \cdot b_3 - r_4 \cdot \bar{\psi}_{s4}^{\chi} \cdot b_4 - r_1 \cdot \bar{\psi}_{s1}^{\chi} \cdot b_1]$$

From Eq(18b),

$$\bar{\psi}_{s3}^{\chi} = \frac{[\bar{\psi}_{s1}^{\chi} \cdot b_1 \cdot (r_2 \cos\alpha_1 - r_1 \cos\alpha_2) + \bar{\psi}_{s4}^{\chi} \cdot b_4 \cdot (r_2 \cos\alpha_4 - r_4 \cos\alpha_2)]}{b_3(r_3 \cos\alpha_2 - r_2 \cos\alpha_3)}$$

From Eq(18c)

$$\bar{\psi}_{s4}^{\chi} = -\bar{\psi}_{s1}^{\chi} \cdot \frac{b_1}{b_4} \cdot \frac{r_3[sin\,\alpha_1 \cos\alpha_2 - sin\,\alpha_2 \cos\alpha_1] + r_2[sin\,\alpha_3 \cos\alpha_1 - sin\,\alpha_1 \cos\alpha_3] + r_1[sin\,\alpha_2 \cos\alpha_3 - sin\,\alpha_3 \cos\alpha_2]}{r_2[sin\,\alpha_3 \cos\alpha_4 - sin\,\alpha_3 \cos\alpha_4] + r_3[sin\,\alpha_4 \cos\alpha_2 - sin\,\alpha_2 \cos\alpha_4] + r_4[sin\,\alpha_2 \cos\alpha_3 - sin\,\alpha_3 \cos\alpha_2]}$$

After determining $\bar{\psi}_{si}^{\chi}$ $(i = 1,2,3,4)$, considering the continuity equations expressed by Eqs. (16) and Eqs.(20) , the remaining 8 coefficients can now be obtained:

From Eqs.(16a)

$$\psi_{s_i}^{\chi}|_{s_i=b_i} = \psi_{s_{i+1}}^{\chi}|_{s_{i+1}=0} \cdot \cos(\alpha_{i+1} - \alpha_i) - \psi_{n_{i+1}}^{\chi}|_{s_{i+1}=0} \cdot sin(\alpha_{i+1} - \alpha_i) \qquad (16a)$$

$$(for\ i = 1,2,3,4\ ;\ 5 \rightarrow 1)$$

$i = 1$ $\psi_{s_1}^{\chi}|_{s_1=b_1} = \psi_{s_2}^{\chi}|_{s_2=0} \cdot \cos(\alpha_2 - \alpha_1) - \psi_{n_2}^{\chi}|_{s_2=0} \cdot sin(\alpha_2 - \alpha_1)$ (16a-1)

$i = 2$ $\psi_{s_2}^{\chi}|_{s_2=b_2} = \psi_{s_3}^{\chi}|_{s_3=0} \cdot \cos(\alpha_3 - \alpha_2) - \psi_{n_3}^{\chi}|_{s_3=0} \cdot sin(\alpha_3 - \alpha_2)$ (16a-2)

$i = 3$ $\psi_{s_3}^{\chi}|_{s_3=b_3} = \psi_{s_4}^{\chi}|_{s_4=0} \cdot \cos(\alpha_4 - \alpha_3) - \psi_{n_4}^{\chi}|_{s_4=0} \cdot sin(\alpha_4 - \alpha_3)$ (16a-3)

$i = 4$ $\psi_{s_4}^{\chi}|_{s_4=b_4} = \psi_{s_1}^{\chi}|_{s_1=0} \cdot \cos(\alpha_1 - \alpha_4) - \psi_{n_1}^{\chi}|_{s_1=0} \cdot sin(\alpha_1 - \alpha_4)$ (16a-4)

Inserting the continuity equations in Eqs.(20a) and Eqs.(20b)

$$\psi_{n_i}^{\chi}|_{s_i=0} = \bar{\psi}_{n_i}^{\chi} + \bar{\psi}_{\theta_i}^{\chi} \cdot \frac{b_i}{2} \qquad (20a)$$

$$\psi_{n_i}^{\chi}|_{s_i=b_i} = \bar{\psi}_{n_i}^{\chi} - \bar{\psi}_{\theta_i}^{\chi} \cdot \frac{b_i}{2} \qquad (20b)$$

Also considering the tangential translations across each wall is constant:

$$\psi_{si}^{\chi}(s_i) = \bar{\psi}_{si}^{\chi} \qquad (15a)$$

Then Eqs.(16a) is now:

$$i = 1 \qquad \bar{\psi}_{s1}^{\chi} = \bar{\psi}_{s2}^{\chi} \cdot \cos(\alpha_2 - \alpha_1) - [\, \bar{\psi}_{n_2}^{\chi} + \bar{\psi}_{\theta_2}^{\chi} \cdot \frac{b_2}{2} \,] \cdot sin(\alpha_2 - \alpha_1) \qquad (16a\text{-}1)$$

$$i = 2 \qquad \bar{\psi}_{s2}^{\chi} = \bar{\psi}_{s3}^{\chi} \cdot \cos(\alpha_3 - \alpha_2) - [\, \bar{\psi}_{n_3}^{\chi} + \bar{\psi}_{\theta_3}^{\chi} \cdot \frac{b_3}{2} \,] \cdot sin(\alpha_3 - \alpha_2) \qquad (16a\text{-}2)$$

$$i = 3 \qquad \bar{\psi}_{s3}^{\chi} = \bar{\psi}_{s4}^{\chi} \cdot \cos(\alpha_4 - \alpha_3) - [\, \bar{\psi}_{n_4}^{\chi} + \bar{\psi}_{\theta_4}^{\chi} \cdot \frac{b_4}{2} \,] \cdot sin(\alpha_4 - \alpha_3) \qquad (16a\text{-}3)$$

$$i = 4 \qquad \bar{\psi}_{s4}^{\chi} = \bar{\psi}_{s1}^{\chi} \cdot \cos(\alpha_1 - \alpha_4) - [\, \bar{\psi}_{n_1}^{\chi} + \bar{\psi}_{\theta_1}^{\chi} \cdot \frac{b_1}{2} \,] \cdot sin(\alpha_1 - \alpha_4) \qquad (16a\text{-}4)$$

The solution for $\bar{\psi}_{n_1}^{\chi}$ and $\bar{\psi}_{\theta_1}^{\chi}$ are calculated in the following procedure:

$$\psi_{n_i}^{\chi}|_{s_i = b_i} = \psi_{s_{i+1}}^{\chi}|_{s_{i+1}=0} \cdot \sin(\alpha_{i+1} - \alpha_i) + \psi_{n_{i+1}}^{\chi}|_{s_{i+1}=0} \cdot cos(\alpha_{i+1} - \alpha_i) \qquad (16b)$$

$$(for\ i = 1,2,3,4\ ;\ 5 \rightarrow 1)$$

For $i = 1$ $\qquad \psi_{n_1}^{\chi}|_{s_1 = b_1} = \psi_{s_2}^{\chi}|_{s_2=0} \cdot \sin(\alpha_2 - \alpha_1) + \psi_{n_2}^{\chi}|_{s_2=0} \cdot cos(\alpha_2 - \alpha_1)$

$$\bar{\psi}_{n_1}^{\chi} - \bar{\psi}_{\theta_1}^{\chi} \cdot \frac{b_1}{2} = \bar{\psi}_{s2}^{\chi} \cdot \sin(\alpha_2 - \alpha_1) + [\, \bar{\psi}_{n_2}^{\chi} + \bar{\psi}_{\theta_2}^{\chi} \cdot \frac{b_2}{2} \,] \cdot cos(\alpha_2 - \alpha_1) \qquad (16b\text{-}1)$$

From Eqs.(16a-1)

$$\bar{\psi}_{n_2}^{\chi} + \bar{\psi}_{\theta_2}^{\chi} \cdot \frac{b_2}{2} = \frac{1}{sin(\alpha_2 - \alpha_1)} \cdot \left[\, \bar{\psi}_{s2}^{\chi} \cdot \cos(\alpha_2 - \alpha_1) - \bar{\psi}_{s1}^{\chi} \,\right]$$

By following similar procedures, the following expressions could be obtained:

$$\bar{\psi}_{n_1}^{\chi} + \bar{\psi}_{\theta_1}^{\chi} \cdot \frac{b_1}{2} = \frac{1}{sin(\alpha_1 - \alpha_4)} \cdot \left[\, \bar{\psi}_{s1}^{\chi} \cdot \cos(\alpha_1 - \alpha_4) - \bar{\psi}_{s4}^{\chi} \,\right]$$

From Eqs.(16b)

$$\psi^{\chi}_{n_1}|_{s_1=b_1} = \bar{\psi}^{\chi}_{n_1} - \bar{\psi}^{\chi}_{\theta_1} \cdot \frac{b_1}{2} = \bar{\psi}^{\chi}_{s_2} \cdot \sin(\alpha_2 - \alpha_1) + \psi^{\chi}_{n_2}|_{s_2=0} \cdot cos(\alpha_2 - \alpha_1)$$

$$\bar{\psi}^{\chi}_{n_1} - \bar{\psi}^{\chi}_{\theta_1} \cdot \frac{b_1}{2} = \bar{\psi}^{\chi}_{s_2} \cdot \sin(\alpha_2 - \alpha_1) + \left[\bar{\psi}^{\chi}_{n_2} + \bar{\psi}^{\chi}_{\theta_2} \cdot \frac{b_2}{2}\right] \cdot cos(\alpha_2 - \alpha_1) \quad (16b\text{-}1)$$

From Eq.(16a-1)

$$\bar{\psi}^{\chi}_{n_2} + \bar{\psi}^{\chi}_{\theta_2} \cdot \frac{b_2}{2} = \frac{1}{sin(\alpha_2 - \alpha_1)} \cdot \left[\bar{\psi}^{\chi}_{s2} \cdot \cos(\alpha_2 - \alpha_1) - \bar{\psi}^{\chi}_{s1}\right]$$

After rearranging the terms:

$$\bar{\psi}^{\chi}_{n_1} - \bar{\psi}^{\chi}_{\theta_1} \cdot \frac{b_1}{2} = \frac{1}{sin(\alpha_2 - \alpha_1)} \cdot \left[\bar{\psi}^{\chi}_{s2} - \bar{\psi}^{\chi}_{s1} \cdot \cos(\alpha_2 - \alpha_1)\right]$$

From Eq.(16a-4), and combining with the above expression

$$\bar{\psi}^{\chi}_{s4} = \bar{\psi}^{\chi}_{s1} \cdot \cos(\alpha_1 - \alpha_4) - \left[\bar{\psi}^{\chi}_{n_1} + \bar{\psi}^{\chi}_{\theta_1} \cdot \frac{b_1}{2}\right] \cdot sin(\alpha_1 - \alpha_4)$$

$$\bar{\psi}^{\chi}_{n_1} + \bar{\psi}^{\chi}_{\theta_1} \cdot \frac{b_1}{2} = \frac{1}{sin(\alpha_2 - \alpha_1)} \left[\bar{\psi}^{\chi}_{s1} \cdot \cos(\alpha_1 - \alpha_4) - \bar{\psi}^{\chi}_{s4}\right] \qquad (16b-2)$$

Setting Eq.(16b-1) = Eq.(16b-2), $\bar{\psi}^{\chi}_{\theta_i}$ and $\bar{\psi}^{\chi}_{n_i}$ (i = 1,2,3,4) could be obtained

$$\bar{\psi}^{\chi}_{\theta_1} = \frac{\left[\bar{\psi}^{\chi}_{s1} \cdot \cos(\alpha_1 - \alpha_4) - \bar{\psi}^{\chi}_{s4}\right]}{b_1 \cdot sin(\alpha_1 - \alpha_4)} - \frac{\left[\bar{\psi}^{\chi}_{s2} - \bar{\psi}^{\chi}_{s1} \cdot \cos(\alpha_2 - \alpha_1)\right]}{b_1 \cdot sin(\alpha_2 - \alpha_1)}$$

$$\bar{\psi}^{\chi}_{\theta_2} = \frac{\left[\bar{\psi}^{\chi}_{s2} \cdot \cos(\alpha_2 - \alpha_1) - \bar{\psi}^{\chi}_{s1}\right]}{b_2 \cdot sin(\alpha_2 - \alpha_1)} - \frac{\left[\bar{\psi}^{\chi}_{s3} - \bar{\psi}^{\chi}_{s2} \cdot \cos(\alpha_3 - \alpha_2)\right]}{b_2 \cdot sin(\alpha_3 - \alpha_2)}$$

$$\bar{\psi}^{\chi}_{\theta_3} = \frac{\left[\bar{\psi}^{\chi}_{s3} \cdot \cos(\alpha_3 - \alpha_2) - \bar{\psi}^{\chi}_{s2}\right]}{b_3 \cdot sin(\alpha_3 - \alpha_2)} - \frac{\left[\bar{\psi}^{\chi}_{s4} - \bar{\psi}^{\chi}_{s3} \cdot \cos(\alpha_4 - \alpha_3)\right]}{b_3 \cdot sin(\alpha_4 - \alpha_3)}$$

$$\bar{\psi}_{\theta_4}^{\chi} = \frac{\left[\bar{\psi}_{s4}^{\chi} \cdot \cos(\alpha_4 - \alpha_3) - \bar{\psi}_{s3}^{\chi}\right]}{b_4 \cdot sin(\alpha_4 - \alpha_3)} - \frac{\left[\bar{\psi}_{s1}^{\chi} - \bar{\psi}_{s4}^{\chi} \cdot \cos(\alpha_1 - \alpha_4)\right]}{b_4 \cdot sin(\alpha_1 - \alpha_4)}$$

$$\bar{\psi}_{n_1}^{\chi} = \frac{\left[\bar{\psi}_{s1}^{\chi} \cdot \cos(\alpha_1 - \alpha_4) - \bar{\psi}_{s4}^{\chi}\right]}{2sin(\alpha_1 - \alpha_4)} - \frac{\left[\bar{\psi}_{s2}^{\chi} - \bar{\psi}_{s1}^{\chi} \cdot \cos(\alpha_2 - \alpha_1)\right]}{2sin(\alpha_2 - \alpha_1)}$$

$$\bar{\psi}_{n_2}^{\chi} = \frac{\left[\bar{\psi}_{s2}^{\chi} \cdot \cos(\alpha_2 - \alpha_1) - \bar{\psi}_{s1}^{\chi}\right]}{2sin(\alpha_2 - \alpha_1)} - \frac{\left[\bar{\psi}_{s3}^{\chi} - \bar{\psi}_{s2}^{\chi} \cdot \cos(\alpha_3 - \alpha_2)\right]}{2sin(\alpha_3 - \alpha_2)}$$

$$\bar{\psi}_{n_3}^{\chi} = \frac{\left[\bar{\psi}_{s3}^{\chi} \cdot \cos(\alpha_3 - \alpha_2) - \bar{\psi}_{s2}^{\chi}\right]}{2sin(\alpha_3 - \alpha_2)} - \frac{\left[\bar{\psi}_{s4}^{\chi} - \bar{\psi}_{s3}^{\chi} \cdot \cos(\alpha_4 - \alpha_3)\right]}{2sin(\alpha_4 - \alpha_3)}$$

$$\bar{\psi}_{n_4}^{\chi} = \frac{\left[\bar{\psi}_{s4}^{\chi} \cdot \cos(\alpha_4 - \alpha_3) - \bar{\psi}_{s3}^{\chi}\right]}{2sin(\alpha_4 - \alpha_3)} - \frac{\left[\bar{\psi}_{s1}^{\chi} - \bar{\psi}_{s4}^{\chi} \cdot \cos(\alpha_1 - \alpha_4)\right]}{2sin(\alpha_1 - \alpha_4)}$$

A general form of $\bar{\psi}_{\theta_i}^{\chi}$ and $\bar{\psi}_{n_i}^{\chi}$ at i[th] wall can be expressed as:

$$\bar{\psi}_{\theta_i}^{\chi} = \frac{\left[\bar{\psi}_{s_i}^{\chi} \cdot \cos(\alpha_i - \alpha_{i-1}) - \bar{\psi}_{s_{i-1}}^{\chi}\right]}{b_i \cdot sin(\alpha_i - \alpha_{i-1})} - \frac{\left[\bar{\psi}_{s_{i+1}}^{\chi} - \bar{\psi}_{s_i}^{\chi} \cdot \cos(\alpha_{i+1} - \alpha_i)\right]}{b_i \cdot sin(\alpha_{i+1} - \alpha_i)}$$

$$\bar{\psi}_{n_i}^{\chi} = \frac{\left[\bar{\psi}_{s_i}^{\chi} \cdot \cos(\alpha_i - \alpha_{i-1}) - \bar{\psi}_{s_{i-1}}^{\chi}\right]}{2sin(\alpha_i - \alpha_{i-1})} - \frac{\left[\bar{\psi}_{s_{i+1}}^{\chi} - \bar{\psi}_{s_i}^{\chi} \cdot \cos(\alpha_{i+1} - \alpha_i)\right]}{2sin(\alpha_{i+1} - \alpha_i)}$$

With the 12 constants known, the distortion function can be plotted as Fig.3.4 using Eq.(15), Eq.(19) and Eq.(22)

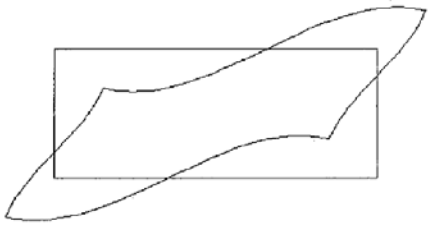

Fig. 3.4 - The distorted shape of the cross-section using the distortion function

3.3 One-Dimensional Analysis

The potential energy can be expressed as :

$$\Pi = \frac{1}{2}\int \sigma_{ij}\cdot\epsilon_{ij}\,dV - \int(p\cdot\tilde{u}_z + q\cdot\tilde{u}_s)\,dV \tag{23}$$

Where p and q are the external loads in the axial and tangential directions.

$$\Pi = \frac{1}{2}\int\{aE_1U'^2 + cE_1\chi^2 + G(b_1U^2 + b_1^*\theta'^2 + b_5\chi'^2) + 2G(b_2U\theta' + b_3U\chi' + b_4\theta'\chi')\}dz - \int(p_1U + q_1\theta + q_2\chi)dz \tag{24}$$

Constants $a, b_1, b_1^*, b_2, b_3, b_4, b_5$ *and* c are

$$a = \int_A (\psi_z^U)^2\,dA = \frac{h^2\cdot b^2\cdot t\cdot(h-b)^2}{2(h+b)}$$

$$b_1^* = \int_A (\psi_s^\theta)^2\,dA = \frac{b\cdot h\cdot t\cdot(b+h)}{2}$$

$$b_1 = \int_A \left(\frac{d\psi_z^U}{ds}\right)^2 dA = \frac{h\cdot b\cdot t\cdot(h-b)^2}{2(h+b)}$$

$$b_2 = \int_A \left(\psi_s^\theta\cdot\frac{d\psi_z^U}{ds}\right)^2 dA = \frac{b\cdot h\cdot t\cdot(h-b)^2}{2(h+b)}$$

$$b_3 = \int_A \left(\psi_s^\chi\cdot\frac{d\psi_z^U}{ds}\right) dA = \bar{\psi}_{s1}^\chi\cdot\frac{2\cdot h\cdot t\cdot(h-b)}{(h+b)}$$

$$b_4 = \int_A (\psi_s^\theta\cdot\psi_z^\chi)\,dA = 0$$

$$b_5 = \int_A \left(\psi_s^{\chi}\right)^2 dA = \ (\bar{\psi}_{s1}^{\chi})^2 \cdot (h+b)$$

$$c = \int_A n^2 \left(\frac{d^2\ \psi_{n_i}^{\chi}}{ds_i{}^2}\right)^2 dA$$

$$= \sum_{i=1}^{4} t^3 \left\{ \left(\frac{\beta_{i(i+1)} + \beta_{i(i)} + 2\bar{\psi}_{\theta_i}^{\chi}}{b_i}\right)^2 + \frac{\left(\beta_{i(i+1)} + \beta_{i(i)} + 2\bar{\psi}_{\theta_i}^{\chi}\right)\left(-\beta_{i(i+1)} - 2\beta_{i(i)} - 3\bar{\psi}_{\theta_i}^{\chi}\right)}{b_i} + \frac{\left(-\beta_{i(i+1)} - 2\beta_{i(i)} - 3\bar{\psi}_{\theta_i}^{\chi}\right)^2}{3b_i} \right\}$$

where $p_1, q_1\ and\ q_2$ are one dimensional load terms defined as

$$p_1 = \int_A p\ \psi_z^U\ dA$$

$$q_1 = \int_A q\ \psi_s^{\theta}\ dA$$

$$q_2 = \int_A q\ \psi_s^{\chi}\ dA$$

Invoking the stationary condition on Π in Eq.(24) yields the following governing equations:

$$-E_1 a U'' + Gb_1 U + Gb_2 \theta' + Gb_3 \chi' = 0 \qquad (25a)$$

$$-Gb_2 U' - Gb_1^{*} \theta'' - Gb_4 \chi'' = 0 \qquad (25b)$$

$$-Gb_3 U' - Gb_4 \theta'' - Gb_5 \chi'' + E_1 c \chi = 0 \qquad (25c)$$

In the first variation of Π, after integration, the boundary terms give the stress resultants:

$$H \equiv \int_A \sigma_{zs}\psi_s^{\theta}\ dA = G(b_1^*\theta' + b_2 U + b_4\chi')\quad (26a)$$

$$B \equiv \int_A \sigma_{zs}\psi_z^{U}\ dA = E_1 a U' \qquad (26b)$$

$$Q \equiv \int_A \sigma_{zs}\psi_s^{\chi}\ dA = G(b_5\chi' + b_3 U + b_4\theta')\quad (26c)$$

Note: *H*,*B* and *Q* are the energy conjugates of $\Theta, U, and\ \chi, respectively$

3.4 Finite Element Theory

Standard two-node displacement-based C^0 continuous finite element approach is used:

$$Kd = P + Q \quad (27)$$

Where the nodal displacement $d = \{\Theta_1 \;\; U_1 \;\; \chi_1 \;\; \Theta_2 \; U_2 \; \chi_2 \}^T$ (28)

Subscript 1 and 2 denote the node numbers in an element level.

The load vectors P and Q are defined as

$$\boldsymbol{P} = \int_{-1}^{1} \boldsymbol{N}^T \, \boldsymbol{R} \, |j| \, d\xi \quad (29)$$

$$\boldsymbol{Q} = \{\mathrm{H}_1 \;\; B_1 \;\; Q_1 \;\; \mathrm{H}_2 \; B_2 \; Q_2 \}^T \quad (30)$$

The matrix N is the linear shape function matrix defined as

$$\mathbf{N} = \begin{bmatrix} \frac{1}{2}(1-\xi) & 0 & 0 & \frac{1}{2}(1+\xi) & 0 & 0 \\ 0 & \frac{1}{2}(1-\xi) & 0 & 0 & \frac{1}{2}(1+\xi) & 0 \\ 0 & 0 & \frac{1}{2}(1-\xi) & 0 & 0 & \frac{1}{2}(1+\xi) \end{bmatrix} \quad (31)$$

ξ in Eq.(29) is the dimensionless coordinate:

$$\xi = \frac{2z - (z_1 + z_2)}{z_2 - z_1}$$

Where $z_1 \; and \; z_2$ are the axial coordinate of the beam elements and $l = z_2 - z_1$, Jacobian

$$\mathrm{J} = l/2$$

$$\boldsymbol{R} = \{q_1 \;\; p_1 \;\; q_2\}^T \quad (32)$$

Stiffness Matrix K :

$$\mathbf{K} = \begin{bmatrix} G\frac{b_1^*}{l} & -G\frac{b_2}{2} & G\frac{b_4}{l} & -G\frac{b_1^*}{l} & -G\frac{b_2}{2} & -G\frac{b_4}{l} \\ & E_1\frac{a}{l} + G\frac{b_1 l}{3} & -G\frac{b_3}{2} & G\frac{b_2}{2} & -E_1\frac{a}{l} + G\frac{b_1 l}{6} & G\frac{b_3}{2} \\ & & G\frac{b_5}{l} + E_1\frac{cl}{3} & -G\frac{b_4}{l} & -G\frac{b_3}{2} & -G\frac{b_5}{l} + E_1\frac{cl}{6} \\ & & & G\frac{b_1^*}{l} & G\frac{b_2}{2} & G\frac{b_4}{l} \\ & \text{—sym—} & & & E_1\frac{a}{l} + G\frac{b_1 l}{3} & G\frac{b_3}{2} \\ & & & & & G\frac{b_5}{l} + E_1\frac{cl}{3} \end{bmatrix}.$$

Chapter 4 Finite element modeling

In this chapter, a number of cases were studied and the result by the present method were compared to the work by previous researchers and the existing F.E.M. computer program Abaqus using 3-D shell element models. Concentrated unsymmetrical loading and uniformly-distributed unsymmetrical loading were applied to models with different dimensions and boundary conditions to study the behavior of the thin-walled box beam under torsional loading.

The field variables including twisting, warping and distortion displacements, the direct warping and distortional (transverse bending) stresses were calculated. The results of Model1 to Model4 using present Method were compared with the F.E.M. software ABAQUS, whilst Model 5 studied the behavior of a thicker cross-section compared to Model1 and Model6 was applied with a pair of uniformly-distributed loads.

4.1 Model1-Cantilever box beam subjected to pair of opposite concentrated loads

Model1 was established referring to the experimental and numerical analysis by Boswell & Zhang (1985) and the asymptotic solutions by Balch & Steele (1987). In the experiment carried out by Boswell & Zhang (1985), a straight cantilever single-cell steel box beam was applied with a pair of opposite point loads at tip ends to form the concentrated torque (P = 4905N, T = 1471.5Nm). The analytic solutions by Balch & Steele(1987) agrees with Boswell & Zhang(1985).

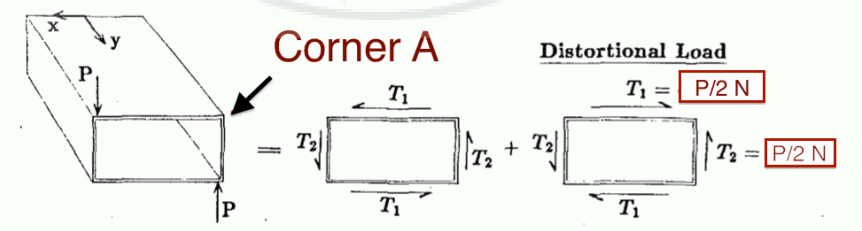

Fig. 4.1.1 - Concentrated loading and the top right corner A

The opposite concentrated loads P= 4905N can be decomposed into two types of loading , as shown in Fig.4.1.1, the torsional load and the distortional load which results

in twisting and distortion, respectively. The 3-Dimesional displacements of Corner A at the top right corner were calculated for convenience, while the overall deformations of the whole cross-section would be shown in the following section for Model1.

Modeling in ABAQUS (F.E.M.)

Preliminary Setting

- 3-D shell , deformable, planar, Standard S4R elements
- E = 196.2 kN/mm^2
- G = 77 kN/mm^2
- v = 0.27
- Flanges width = 300mm, webs height = 150mm
- Uniform Thickness t = 3.18 mm
- Beam Length = 1500 mm

Boundary and Loading Condition

- Fixed-support at one end
- Each of the concentrated load = 4905N and -4905N in y-direction

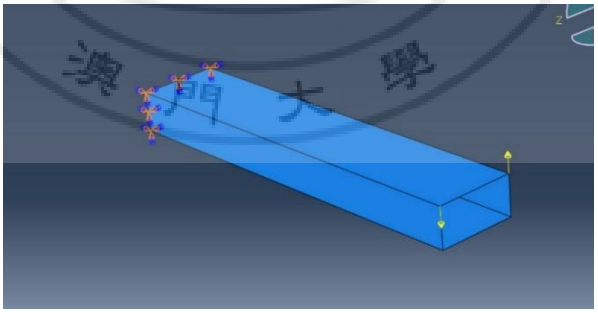

Fig. 4.1.2 - Boundary and Loading condition of Model1

Meshing

The numbers of elements used in F.E.M. software and the developed present Program were chosen by the following comparison, the 3-dimensional displacements of top right corner A at the free end:

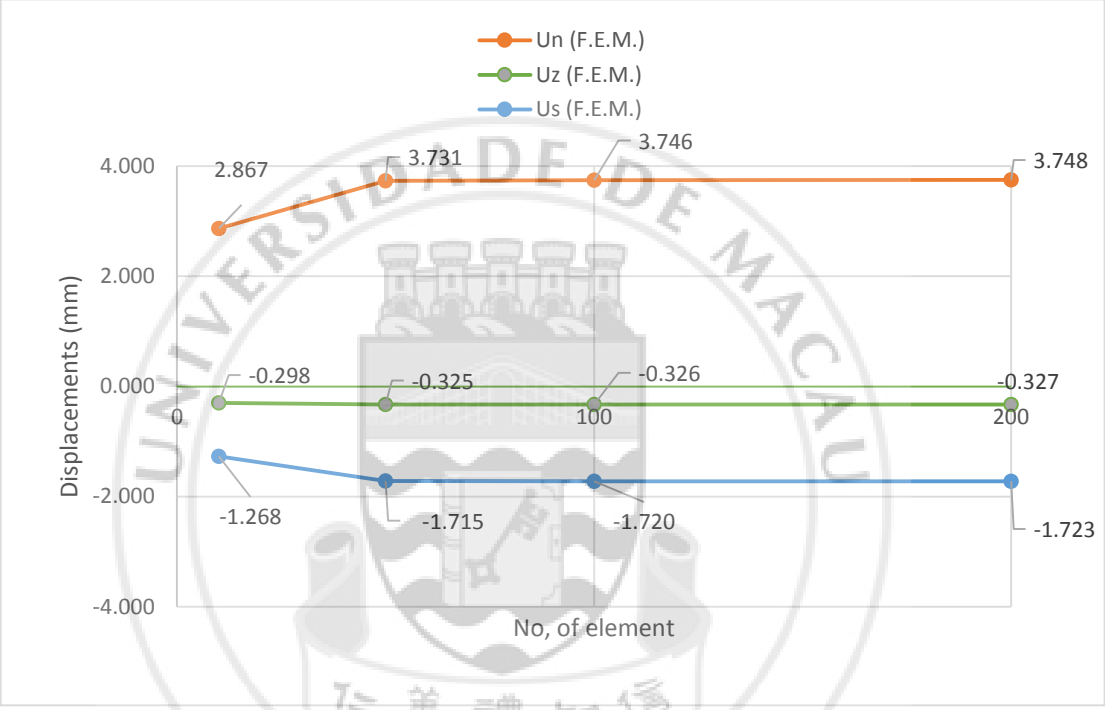

Fig. 4.1.3 – 3-dimensional displacements of corner A with different number of elements

The number of elements used for the F.E.M. Model in the longitudinal direction was **200**, the element size is 7.5mmx7.5mm with thickness equals to 3.18mm as shown in Fig.4.1.5. The largest difference of the three-dimensional displacements between using number of elements of 100 and 200 is **0.306 %** which should provide enough accuracy of the analysis.

To be consistent, the number of elements used in the present method is also 200 in the longitudinal direction and the size of element is the same.

Since the present method adopts only 1-dimesional Finite element theory, the meshing of the cross-section does not affect the accuracy of the analysis but only the continuity of the distortion function. Fig.4.1.4 shows that the comparison of three-dimensional displacements and the number of elements used. Note that Model2 and Model3 use the same number of elements as Model1, the detail of meshing is only discussed in this section.

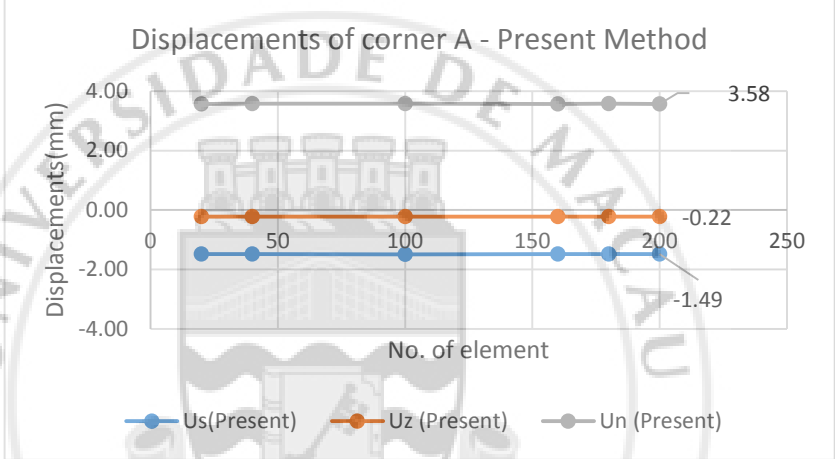

Fig. 4.1.4. – 3-dimensional displacements of corner A with different number of elements

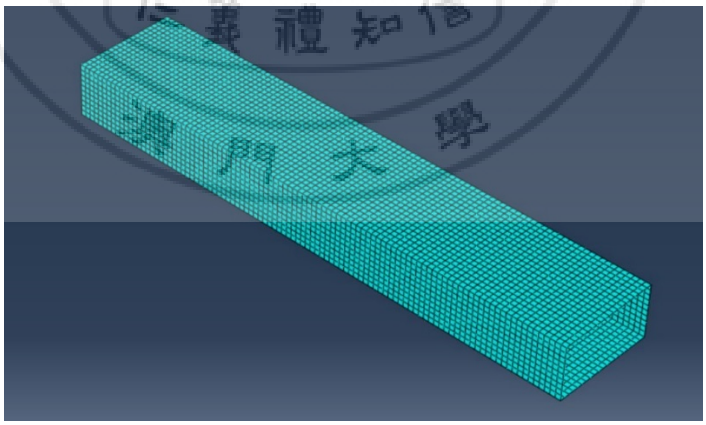

Fig. 4.1.5. - Meshing of Model1

4.2 Model2- Fixed-supported box beam subjected to pair of opposite concentrated loads

Model2 refers to the Model1 with the same dimensions, but the Boundary conditions varied. Fixed supports were provided at both ends of the beam, restricted from any displacement at its end. The pair of opposite point loads was applied at the mid-span of the beam.

Preliminary Setting

- 3-D shell , deformable, planar, Standard S4R elements
- E = 196.2 kN/mm^2 ,G = 77 kN/mm^2 , v = 0.27
- Flanges width = 300mm, webs height = 150mm
- Uniform Thickness t = 3.18 mm
- Beam Length = 1500 mm

Boundary and Loading Condition

- Fixed-support at both ends
- Each of the concentrated load = $\pm$ 10000N in y-direction at mid-span

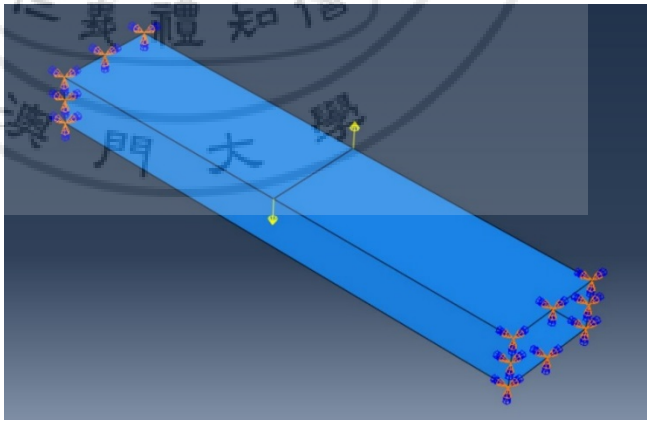

Fig. 4.2.1. - Loading and Boundary conditions of Model2

Meshing

- 200 elements in the longitudinal direction

- Element size = 7.5mm x 7.5mm x 3.18mm
- The meshing detail can referred to Model1

4.3 Model3 - Cantilever square box beam subjected to pair of opposite concentrated loads

Model3 refers to the Model1 with same boundary conditions but the cross-section is square. The beam was applied with a pair of opposite concentrated loads (P = $\pm$4905 N) same with Model1. The behavior of square-section is to be studied.

Preliminary Setting

- 3-D shell , deformable, planar, Standard S4R elements
- E = 196.2 kN/mm^2 , G = 77 kN/mm^2 , v = 0.27
- Flanges width = 150mm, webs height = 150mm
- Uniform Thickness t = 3.18 mm
- Beam Length = 1500 mm

Boundary and Loading Condition

- Fixed-support at one end
- Each of the distributed load = $\pm$4905N in y-direction

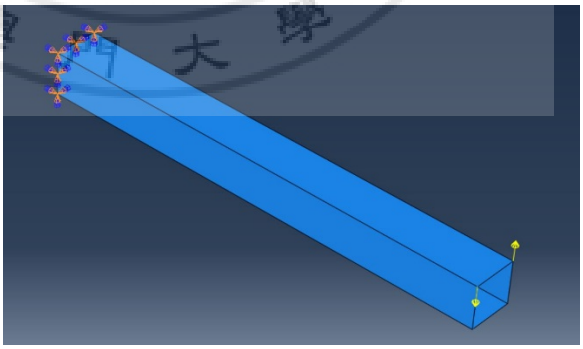

Fig. 4.3.1. - Boundary and Loading conditions of Model 3

Meshing

- 200 elements in the longitudinal direction
- Element size = 7.5mm x 7.5mm x 3.18mm

4.4 Model4-Cantilever box beam subjected to pair of opposite concentrated loads

Model4 refers to the Model1 with same boundary conditions but the Flange length is **100mm** and the web height is **150mm**. The beam was applied with a pair of opposite concentrated loads (P = $\pm$4905 N) same with Model1.

Preliminary Setting

- 3-D shell , deformable, planar, Standard S4R elements
- E = 196.2 kN/mm^2 , G = 77 kN/mm^2 , v = 0.27
- Flanges width = 100mm, webs height = 150mm
- Uniform Thickness t = 3.18 mm
- Beam Length = 1500 mm

Boundary and Loading Condition

- Fixed-support at one end
- Each of the distributed load = $\pm$4905N in y-direction

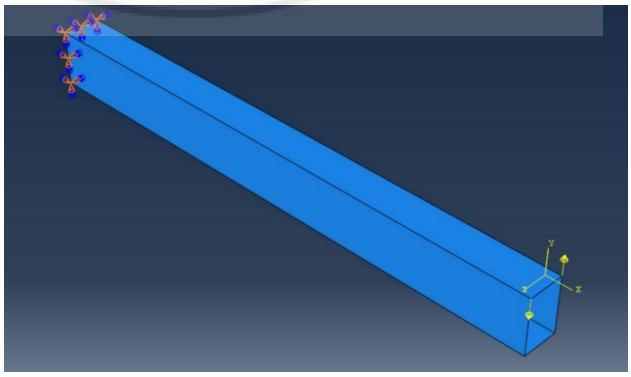

Fig. 4.4.1 - Boundary and Loading conditions of Model 4

Meshing

- 200 elements in the longitudinal direction
- Element size = 7.5mm x 7.5mm x 3.18mm

4.5 Model5-Cantilever box beam subjected to pair of opposite concentrated loads

Preliminary Setting of the present method

- 3-D shell , deformable, planar, Standard S4R elements
- Flanges width = 150mm, webs height = 150mm
- Uniform Thickness t = **6** mm
- Beam Length = 1500 mm

Boundary and Loading Condition of the present method

- Fixed-support at one end
- Each of the concentrated load P = $\pm$4905N in y-direction at free end

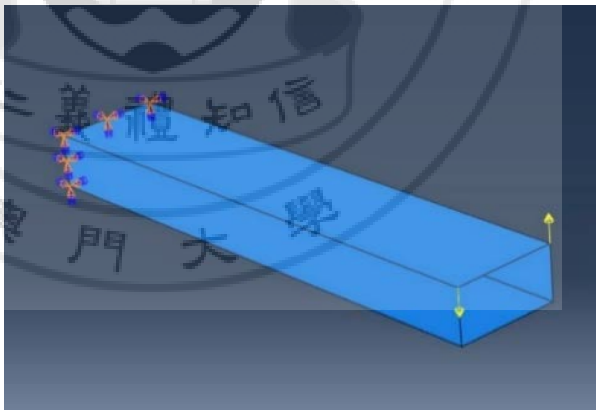

Fig. 4.5.1 - Boundary and Loading Condition

4.6 Model6- Cantilever box beam subjected to pair of opposite distributed loads

Preliminary Setting of the present method

- 3-D shell , deformable, planar, Standard S4R elements
- Flanges width(b) = 300mm, webs height (h) = 150mm
- Uniform Thickness t = 3.18 mm
- Beam Length = 1500 mm

Boundary and Loading Condition of the present method

- Fixed-support at one end
- Each of the uniformly distributed load w = $\pm$3.27N/mm in y-direction along two edges (P = 3.27 x 1500 = 4905N)

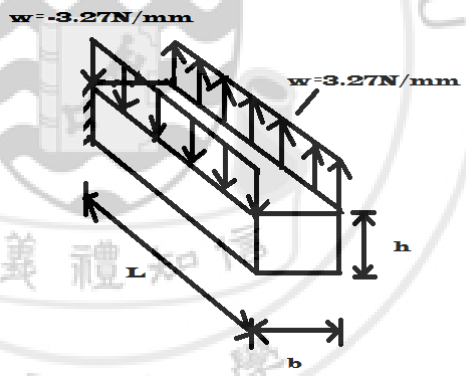

Fig. 4.6.1. - Boundary and loading conditions of Model6

Chapter 5 Result and Discussion

The results to be discussed include the following field variables:

- Tangential displacement of the contour u_s
- Normal displacement of the contour u_n
- Axial displacement of the contour u_z
- Distortion Angle of the cross-section γ_d
- Twisting Angle of the cross-section γ_t
- Direct Warping Stress σ_w
- Distortion (Transverse bending) Stress σ_d

The definition of distortional angle γ_d can be referred to Balch & Steele (1987),

$$\boldsymbol{\gamma_d} = -\frac{u_{s,1}}{b} + \frac{u_{s,4}}{h} \tag{33}$$

Where $u_{s,1}$ and $u_{s,4}$ denote the tangential displacement of contour 1 (top flange) and 4(right web), respectively; b is the width of flange; h is the depth of web.

With the present method, the distortional angle of the beam is compared with the asymptotic solution by Balch & Steele (1987) and numerical solution by Boswell & Zhang (1983). The numerical solution by Boswell & Zhang (1983) was in close agreement with their experimental result, which is not shown here. In Eq.(33), the distortional angle $\boldsymbol{\gamma_d}$ equals to the sum of the ratio of the tangential displacement of the contour over its length, with higher distortional angle, the more the cross-section is distorted. Note that $u_{s,1}$ is positive if it translates from right to left of wall 1, for the loading considered of Model1, following the distortion shape, $u_{s,1}$ has a negative value as

it translates from left to right; $u_{s,4}$ is in a positive sense, as shown in Fig.5.0.1. In the figure, $u_o^I = -u_{s,1}$; $u_O^{II} = -u_{s,4}$.

Distortion Angle Γ :

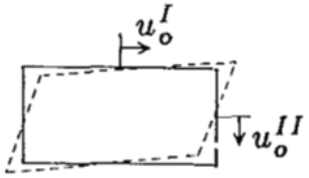

$$\Gamma = \frac{u_o^I}{b} - \frac{u_o^{II}}{a} \quad .$$

Fig.5.0.1 - Distortional angle

The definition of twisting angle γ_t can be referred to Boswell & Zhang (1985) ,

$$\gamma_t = \left(\frac{u_{s,4}}{b} + \frac{u_{s,1}}{h}\right) \qquad (34)$$

Where $u_{s,1}$ and $u_{s,4}$ denote the tangential displacement of contour 1 (top flange) and 4 (right web), respectively; b is the width of flange; h is the depth of web.

The twisting angle is relatively smaller than the distortional angle as it is the difference between the ratio of tangential displacement of the contour over its length. The value of twisting angle simply indicates that how much the cross-section has rotated.

To compare the stress component by warping and distortion, the direct stress component and distortional stress component are as follows:

$$\sigma_w = E_1 \cdot \epsilon_{zz} \qquad (35)$$

$$\sigma_d = E_1 \cdot \epsilon_{ss} \qquad (36)$$

5.1 Model1

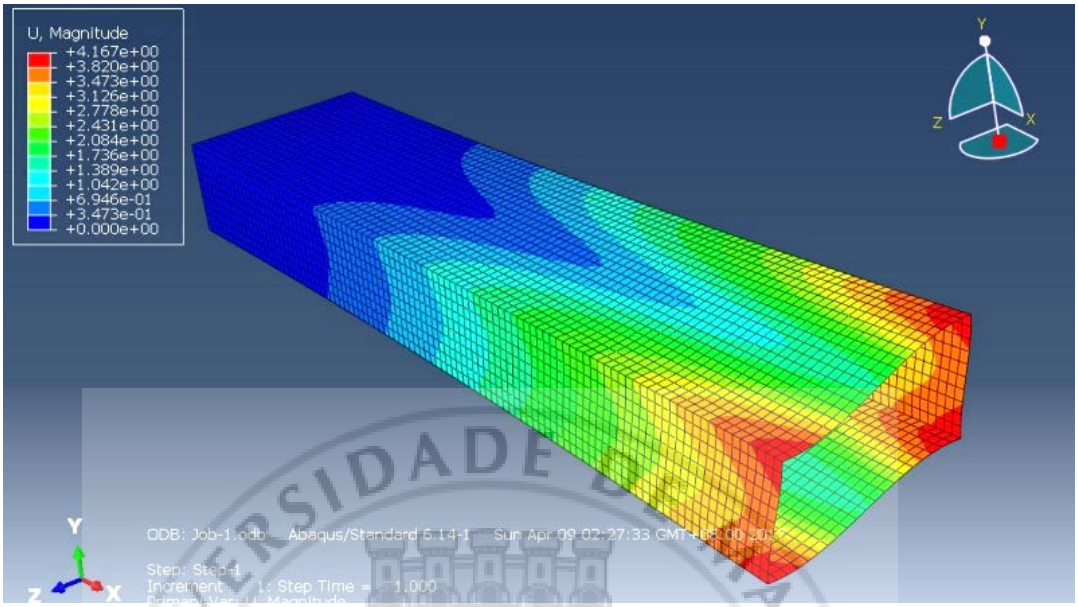

Fig. 5.1.1 - Deformed shape

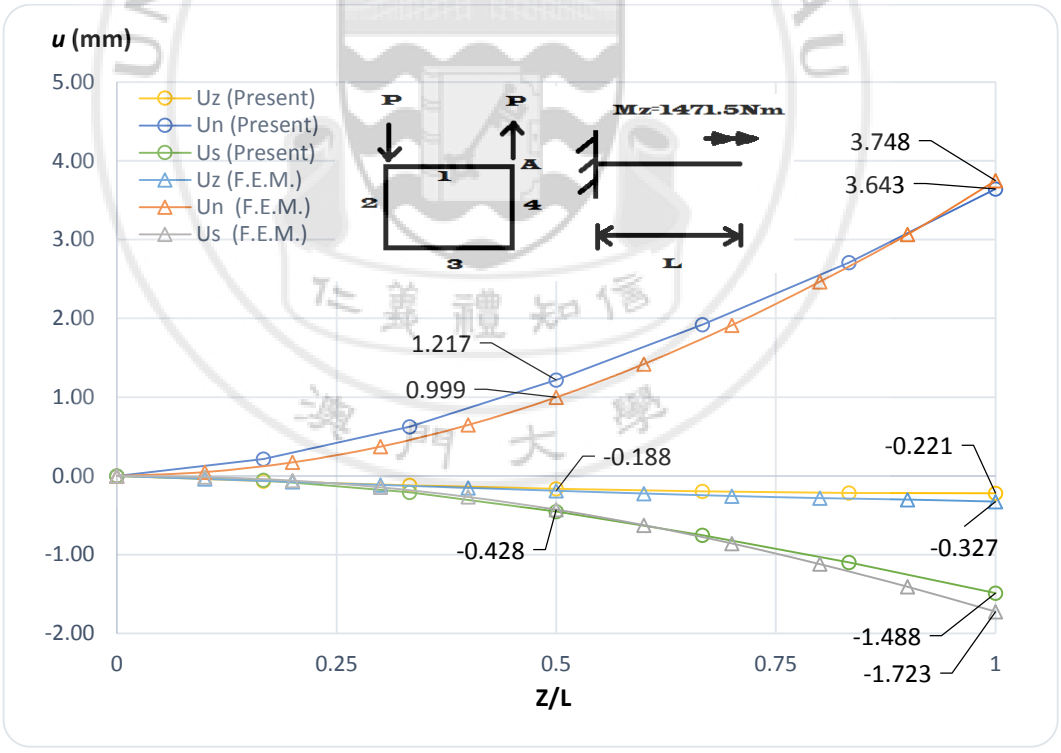

Fig. 5.1.2 – 3-dimensional Displacements of Corner A (L = 1500mm, Mz = 1471.5Nm)

To discuss the result by the present method, firstly the 3-dimesional displacements (u_s, u_n, u_z) of top right corner A were compared with the result by F.E.M. Abaqus model.

Table 5.1 Relative Error of 3-Dimensional Displacements

Max. Displacement	u_n (mm)	u_s (mm)	u_z (mm)
Present Method	3.643	-1.488	-0.221
Abaqus	3.748	-1.723	-0.327
Relative Error	2.3%	13.6%	32.4%

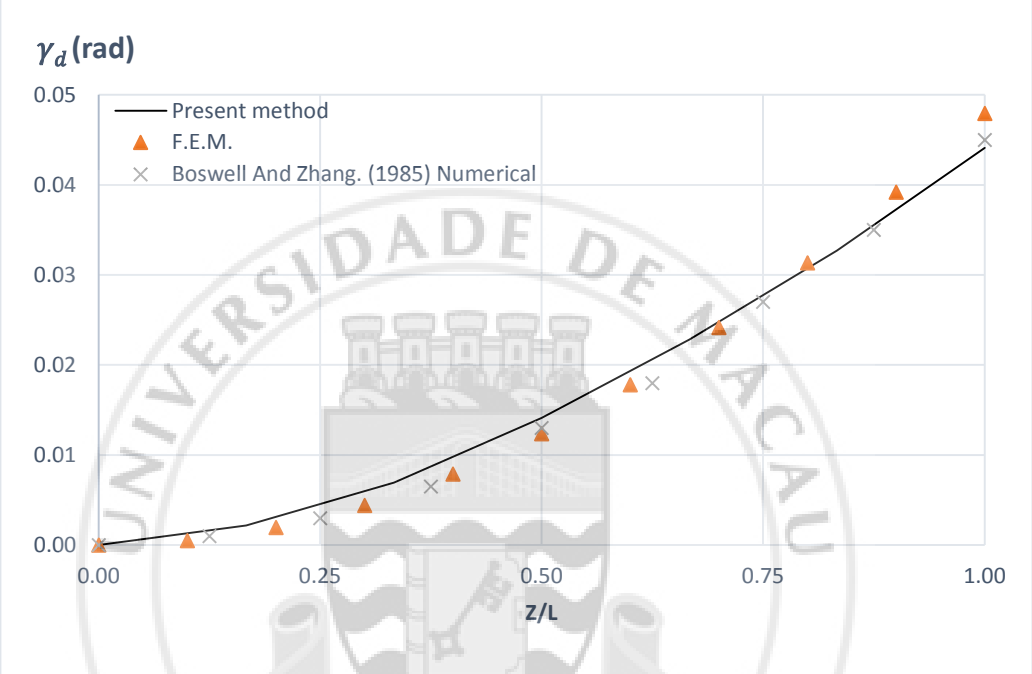

Fig. 5.1.3 - Distortional angle along z-axis, L = 1500mm

As there was only Normal (Vertical) displacement of the top flange at 7/8 span (1312.5mm) provided by the numerical and experimental result by Boswell & Zhang (1985), There is not much reference to compare the spatial displacement of the cross-section but only using the F.E.M. program with shell elements. The present method adopts only one-dimensional analysis while the existing F.E.M. model uses 3-D finite element analysis. However, as a coupled deformation of the vertical and horizontal deflections, the distortional angle shown in Fig.5.1.3 by the present method is in close agreement with Boswell & Zhang (1985) and the F.E.M. model, reflecting a slope-increasing trend as further away from the fixed end under a concentrated torsional loading at the free end.

The vertical displacement distribution along top flange at 7/8span (Fig.5.1.5) is in good agreement with the numerical solution by Boswell & Zhang (1985). Attention should be made that under the distortion deformation, the maximum vertical deflection does not occur right at the corners, as the cubic distortion function proposed by Kim & Kim (1999), with the rotation continuity of the corner considered the maximum deflection occurs near the corners for the flange. On the other hand, the negative u_z indicates the top right corner is compressed while positive value indicates the point is under tension.

The warping displacement of each contour is not shown here, in Fig.5.1.4(a), the warping function for Model1 agrees with the F.E.M. result that it is a linear function and has a maximum value at corners, zero warping at middle of the contour. For convenience, only the warping displacements of top right corner A is compared through the report. The linear distortion and warping stresses profile are also shown in Fig.5.1.4(b) and Fig.5.1.4(c). In the following sections, only stresses at corners will be discussed.

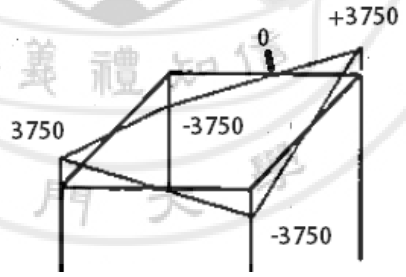

Fig. 5.1.4(a) - Warping function for Model1

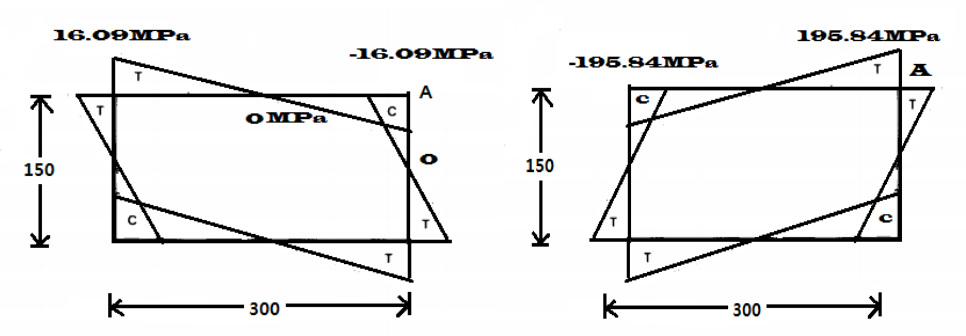

Fig. 5.1.4(b) - Warping Stress at 3l/4(Present) Fig. 5.1.4(c) -Distortional Stress z = L

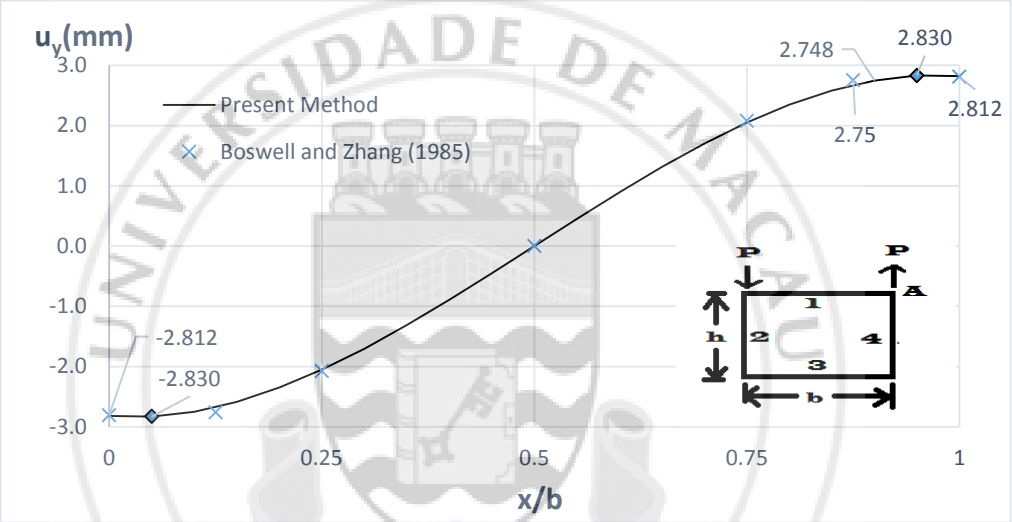

Fig. 5.1.5. - Vertical Displacement distribution along top flange (wall1) at 7/8 span

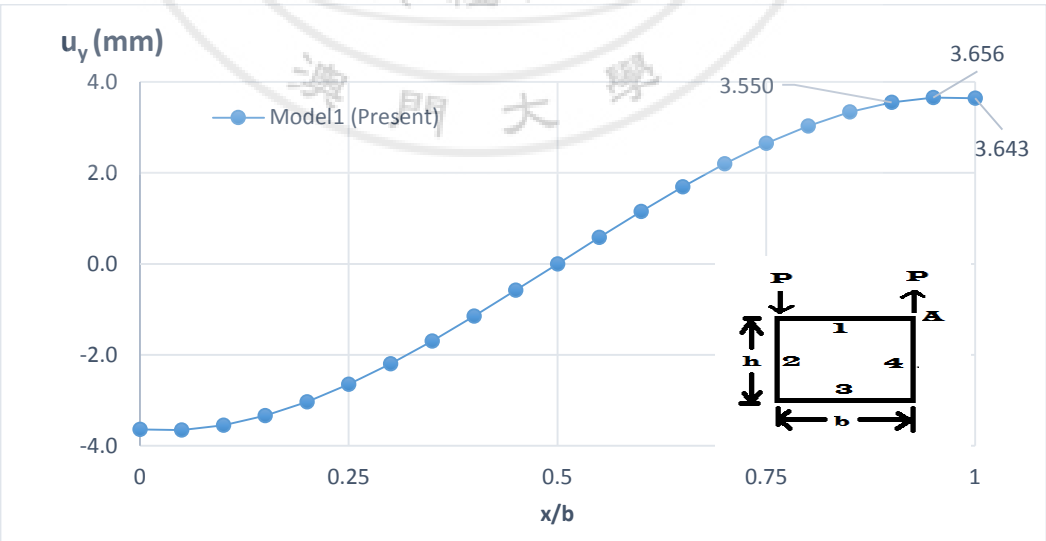

Fig. 5.1.6. - Vertical displacement distribution along top flange (wall1) at free end

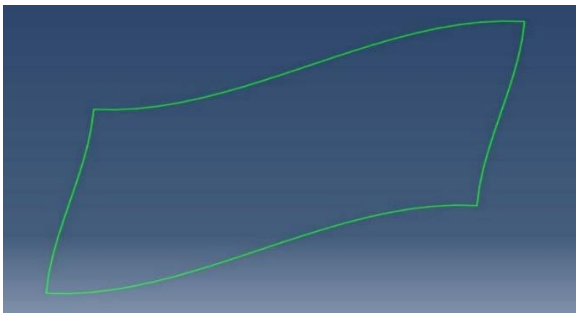

Fig. 5.1.7. - Deformed shape of cross-section at free end

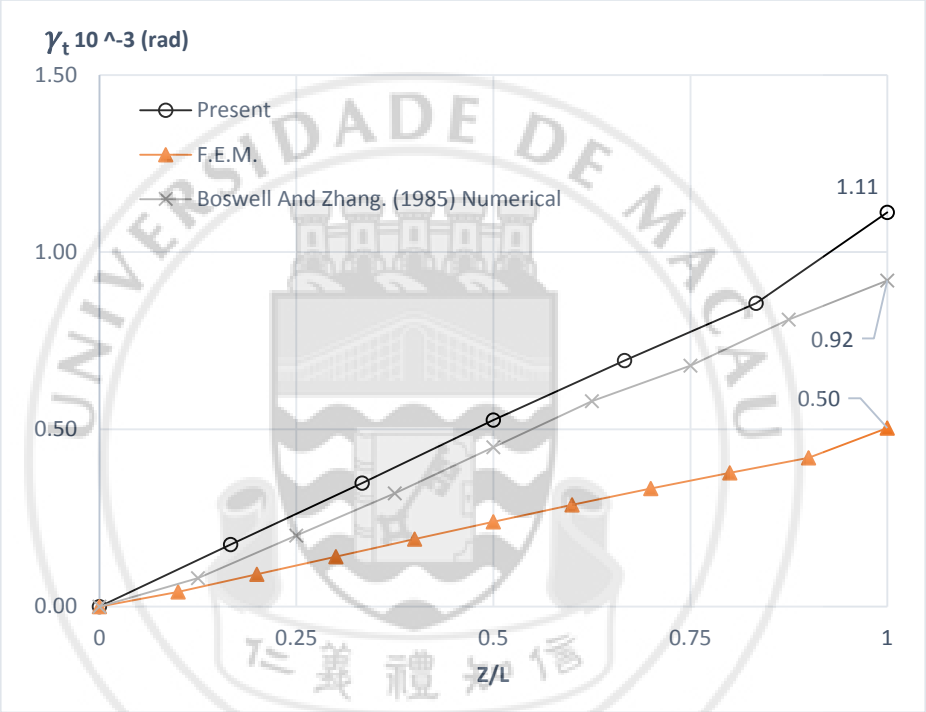

Fig. 5.1.8 - Twisting angle along z-axis, L = 1500mm

The twisting angle (Fig.5.1.8) from F.E.M. model has a relative smaller value compared to the present method, however, the three methods show almost linear increase along the longitudinal axis under concentrated opposite point loads at free end. The critical consideration governing the design of the box beams will be the stress analysis (Fig.5.1.9), the direct warping stress 59.52Mpa(present) and 50Mpa (Balch & Steele (1987)) are maximum at the fixed end and zero at the free end as the beam is free to warp at its end. The distortional stress is 205MPa (present) and -195.84Mpa (Balch & Steele

(1987)) are maximum at the free end and has a flatter slope at first but increases gradually along the beam.

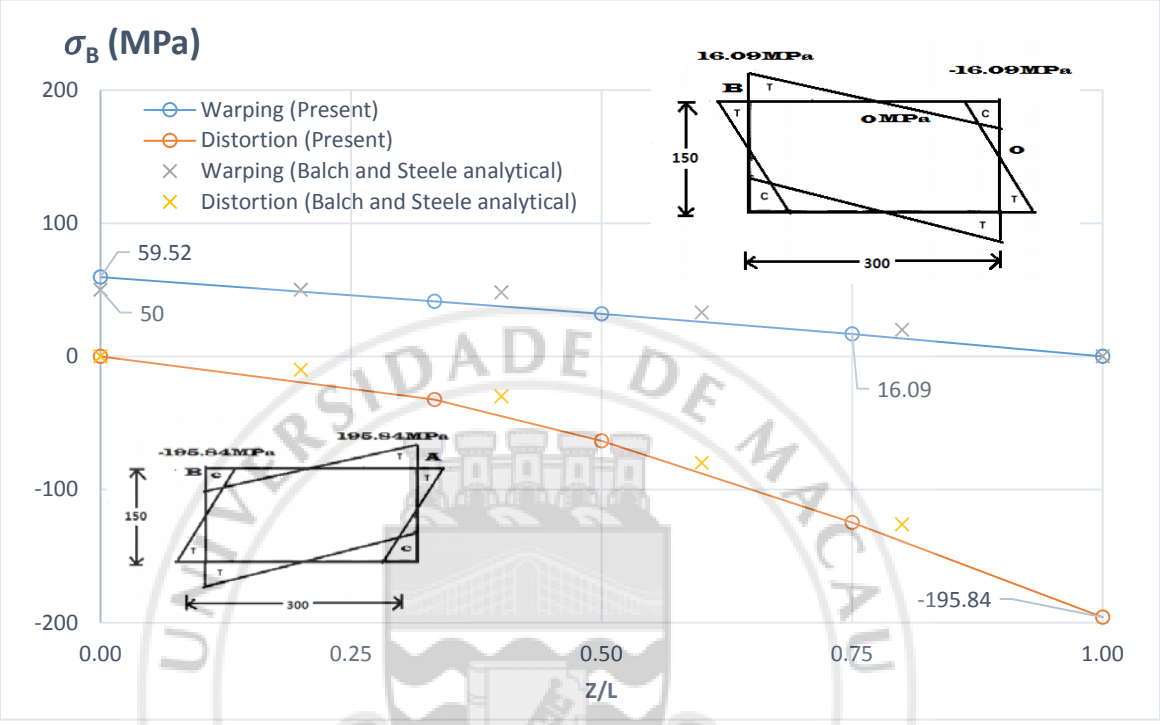

Fig. 5.1.9. - Distortional and warping stress at corner B

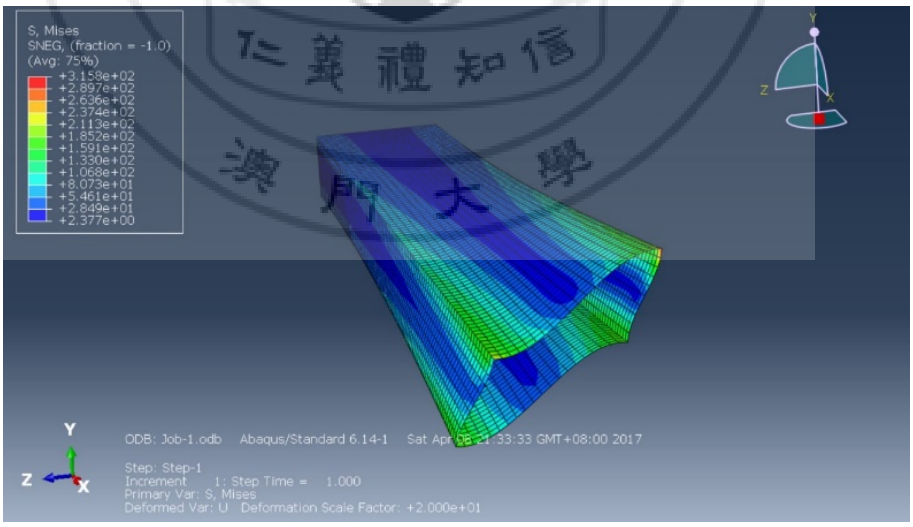

Fig. 5.1.10. - Stress (mises) of the beam

5.2 Model2

With the same dimension as Model1, fixed-supports are provided at both ends.

With the visualization of Fig.5.2.1. The maximum deflection magnitude takes place at mid-span , but only for the distortional deformation (vertical and horizontal), shown in Fig.5.2.2, the warping displacement of the top right corner A is zero at mid-span, but maximum at $l/4$ (compression) and $3l/4$ (tension). Each of the relative error of maximum displacements:

Table 5.2 Relative error of 3-Dimensional displacements

	u_s (mm)	u_n (mm)	u_z (mm)
Present Method	-0.106	0.484	0.016
Abaqus	-0.158	0.459	0.048
Relative error:	32.9%	5.16%	66.6%

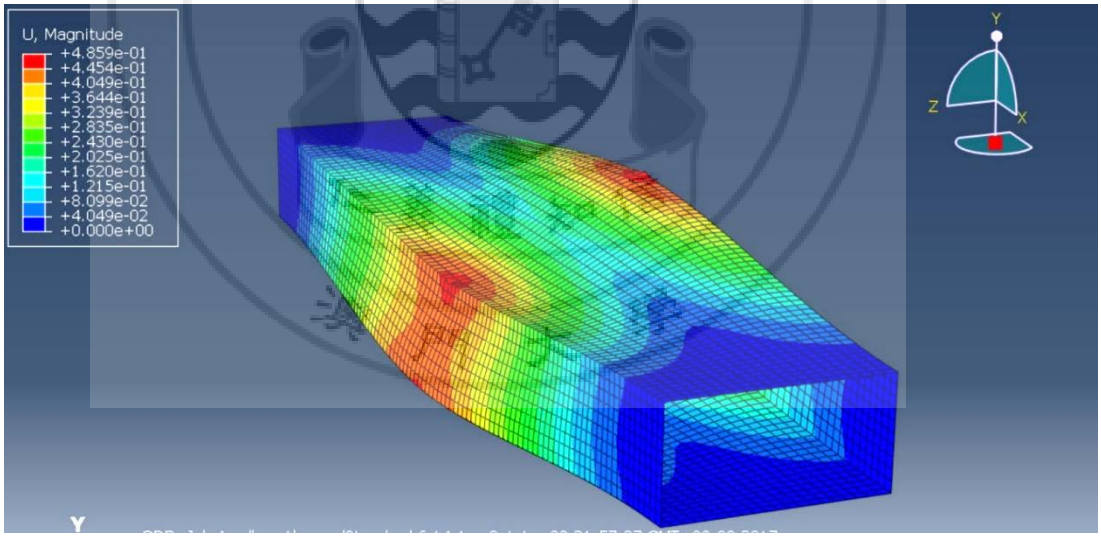

Fig. 5.2.1(a) - Deformed shape of Model2

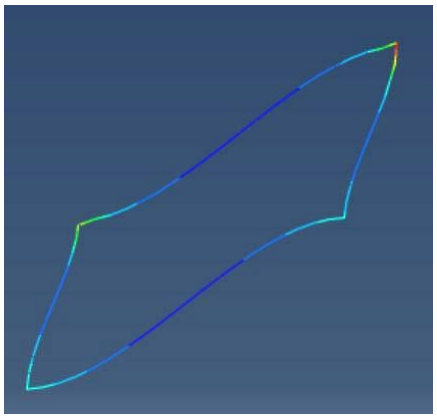

Fig. 5.2.1(b) - Deformed shape of the cross-section at mid-span

Once again, the warping displacement shows a large difference between two methods, but the behavior of deformation is in agreement with the three-dimensional displacements components (Fig.5.2.2) for the present method and F.E.M. analysis.

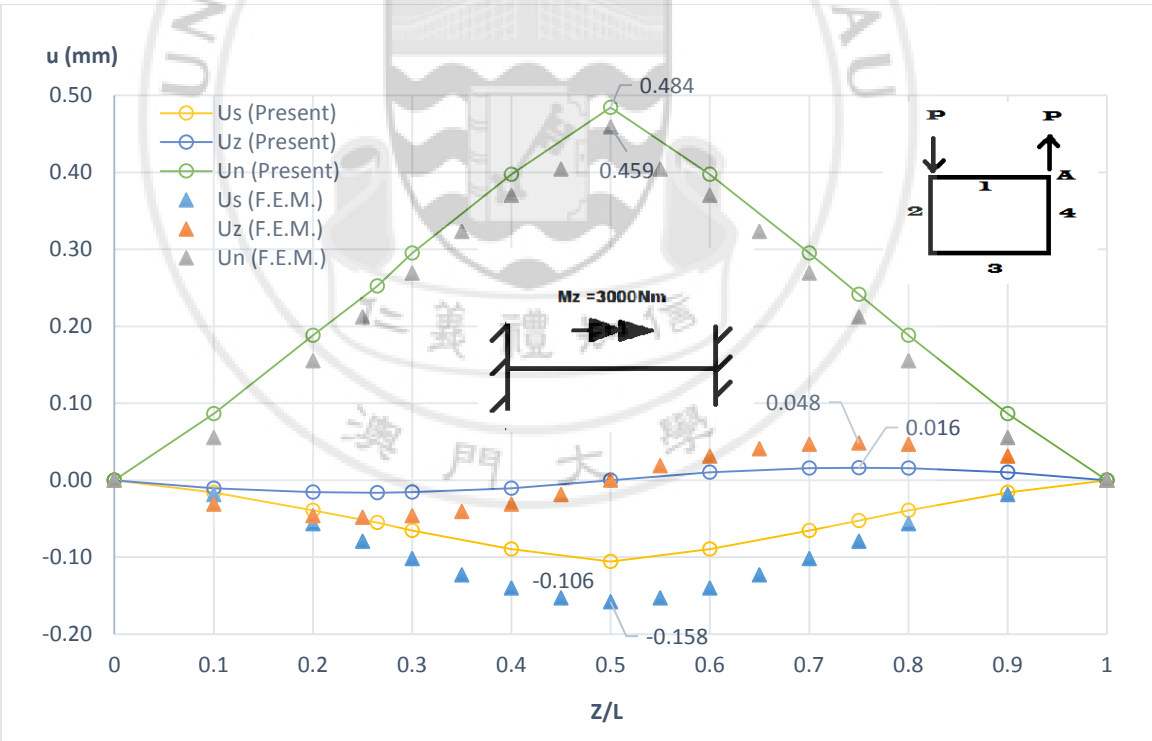

Fig. 5.2.2 – 3-dimesnional displacements of corner A, (Mz = 3000Nm)

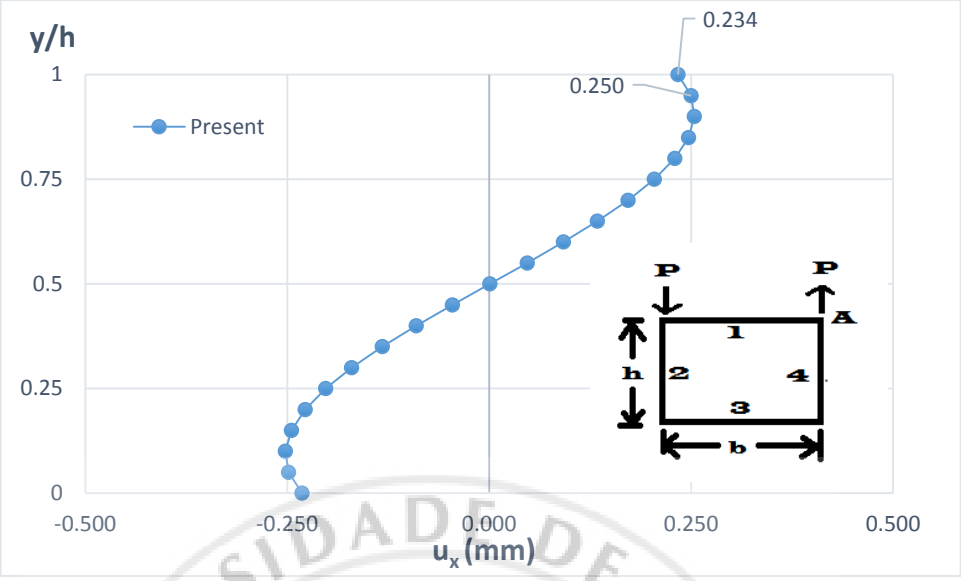

Fig. 5.2.3 - Horizontal displacements (u_n) of the right web (wall4) at mid-span

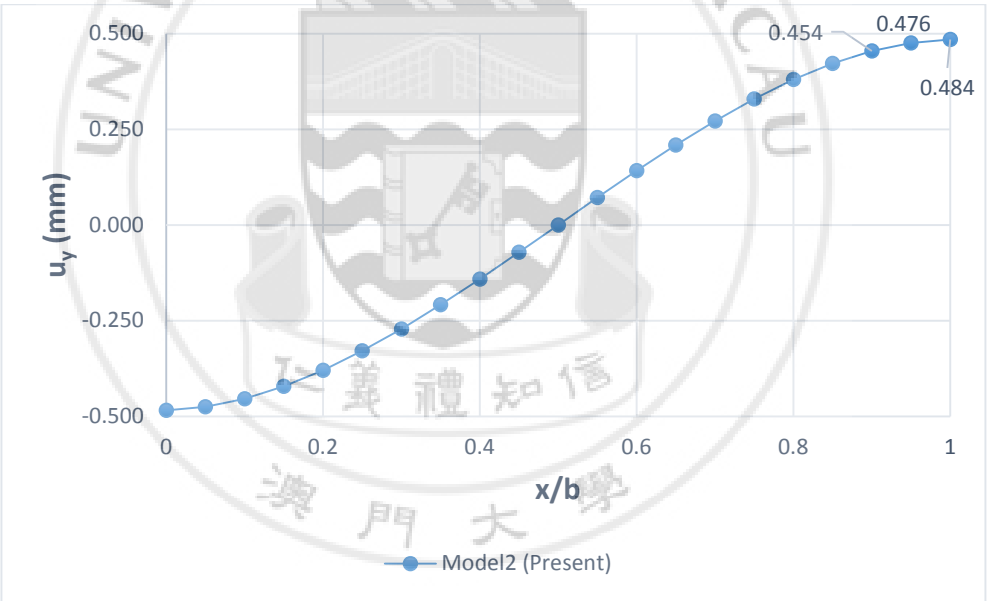

Fig. 5.2.4 - Vertical displacement of top flange at mid-span

The vertical and normal displacement has a maximum value at the corner for this model at mid-span which the warping deformation is zero. The distortional angle has a maximum value of 0.00464(present method) and 0.00517rad (abaqus) at mid-span, and is in agreement with the Abaqus result.

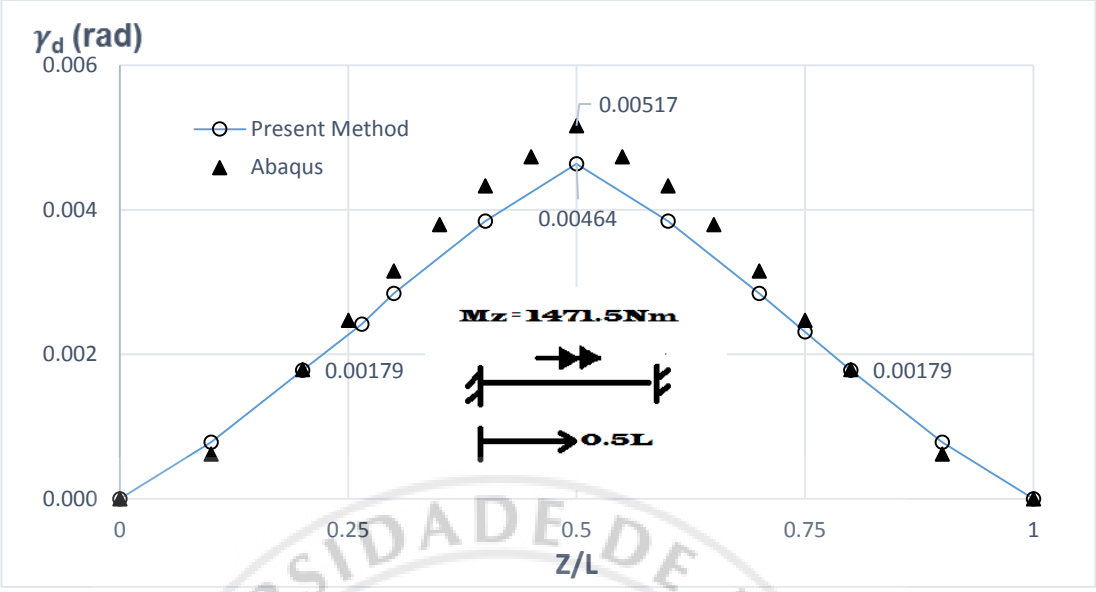

Fig. 5.2.5 - Distortional Angle distribution along z-axis, L = 1500mm

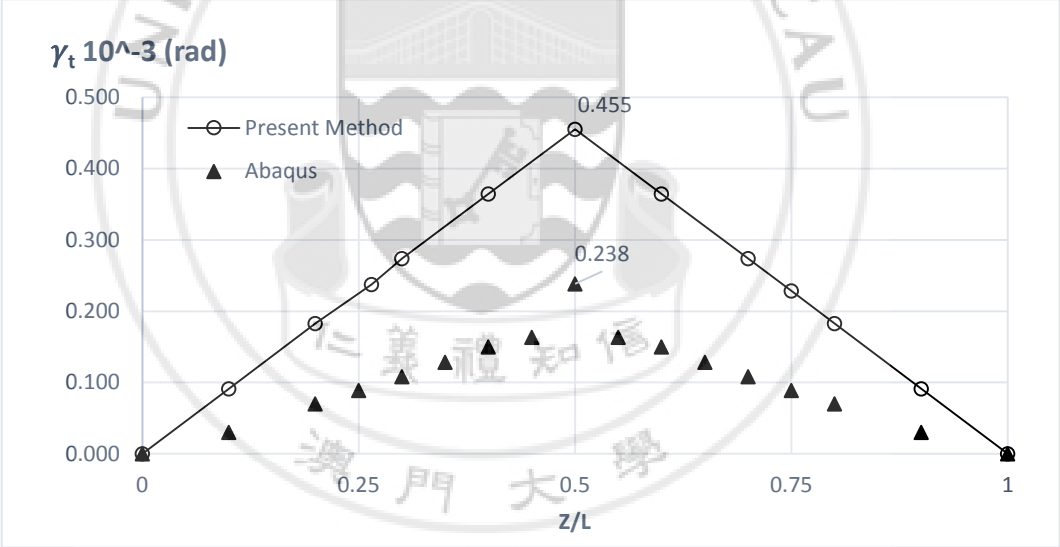

Fig. 5.2.6 - Twisting angle distribution, L = 1500mm

The twisting angle along the beam changes linearly with the present method but a sharp increase at mid-span using F.E.M. Abaqus analysis, the relative error is 47.7 %.

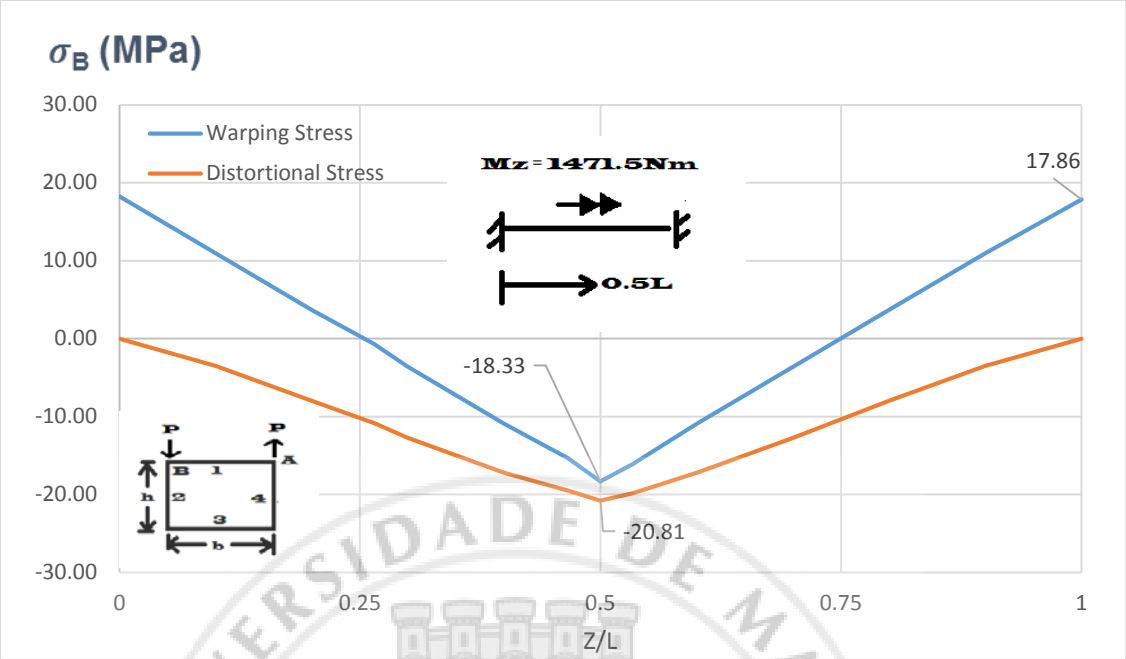

Fig. 5.2.7 - Distortional and warping stress distribution at B

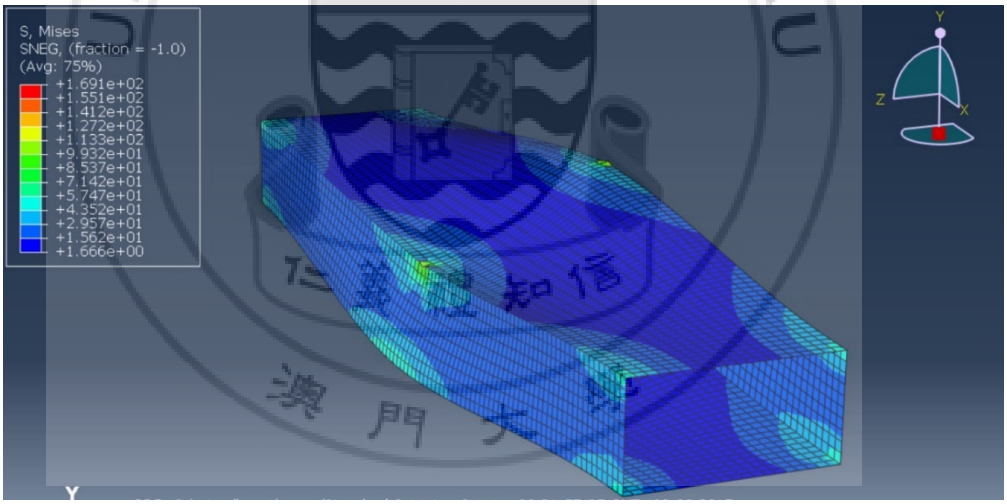

Fig. 5.2.8 - Stress (mises) of the beam

The distribution of the distortional and warping stress is shown in Fig.5.2.7 and Fig.5.2.8, the distortion stress has its critical values at mid-span and at the supports while the warping stress is maximum at the mid-span at which there is not any warping deformations. Both of the stresses change linearly along the beam rather than a curve.

5.3 Model3

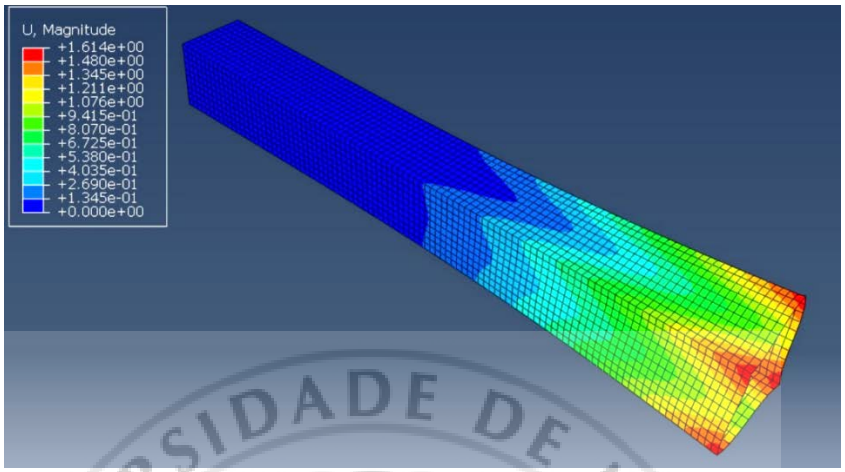

Fig. 5.3.1 - Deformed shape

Table 5.3 Relative error of 3-Dimensional displacements

	u_s (mm)	u_n (mm)	u_z (mm)
Present Method	-0.897	1.324	-0.087
Abaqus	-1.009	1.248	-0.167
Relative error:	11.1%	6.1%	47.9%

With a square cross-section, the axial decay effect of the deflections and stresses are significant than a cross-section with higher flange-web ratio. Under the same pair of opposite point loads, the three-dimensional displacements are smaller than Model 1 which has a wider flange. From Fig.5.3.1 and Fig.5.3.2 the beam deformations almost start from mid-span by the Abaqus result. Furthermore, the distortional angle increases rapidly after mid-span but resulting in 0.03010(rad) which has a relative error of 1.6% compared to the present method (0.02961 rad). The three-dimensional displacements show similar trends but also start to increase further away from the support. With the significant axial decay effect for the square cross-section, Model 4 has a lower flange-width ratio equals to 1:2 to further study the behavior of distortional deformation.

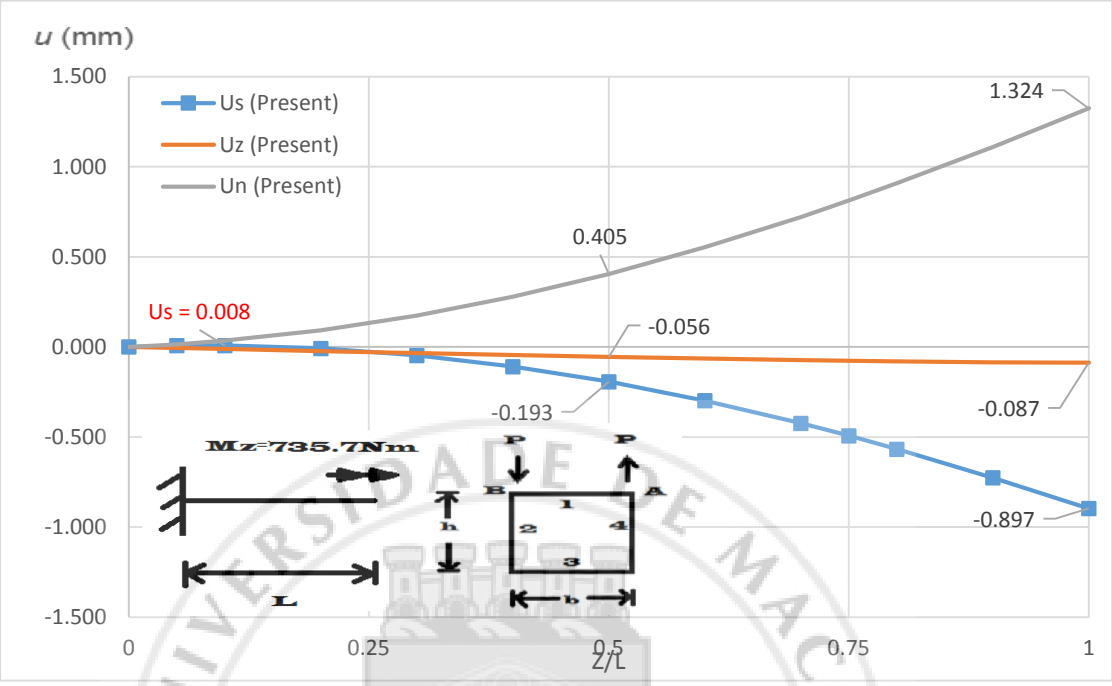

Fig. 5.3.2(a) 3-Dimesional displacements of top right corner A, (L = 1500mm, b=h=150mm)

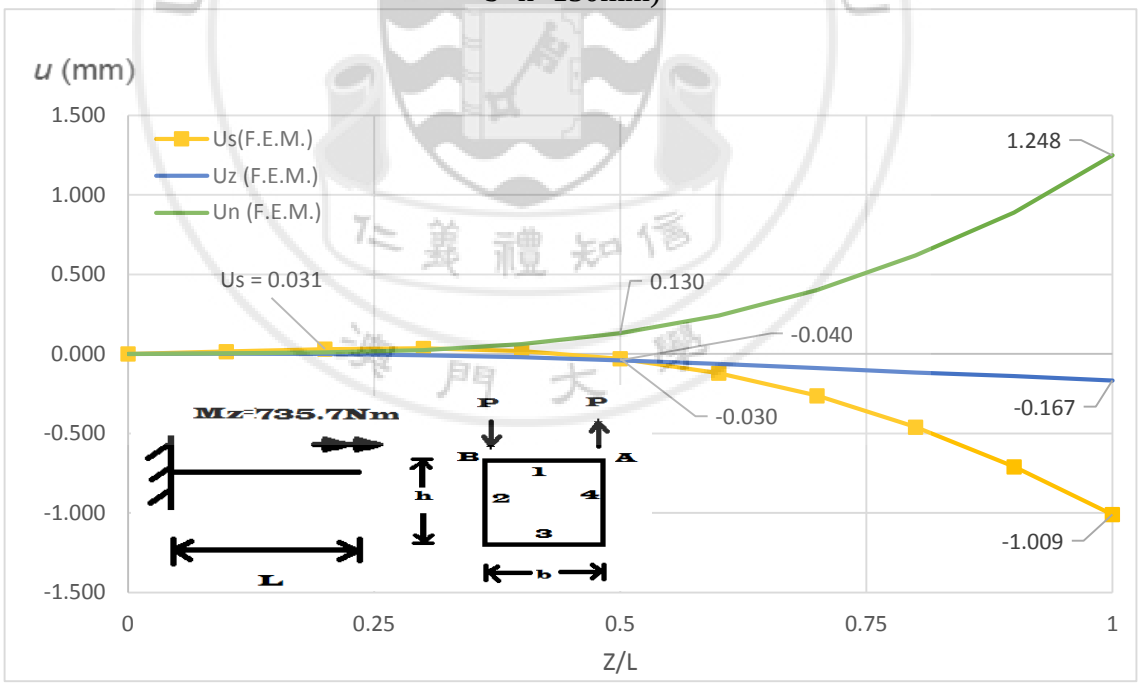

Fig. 5.3.2(b) 3-Dimesional displacements of top right corner A, (L = 1500mm, b=h=150mm)

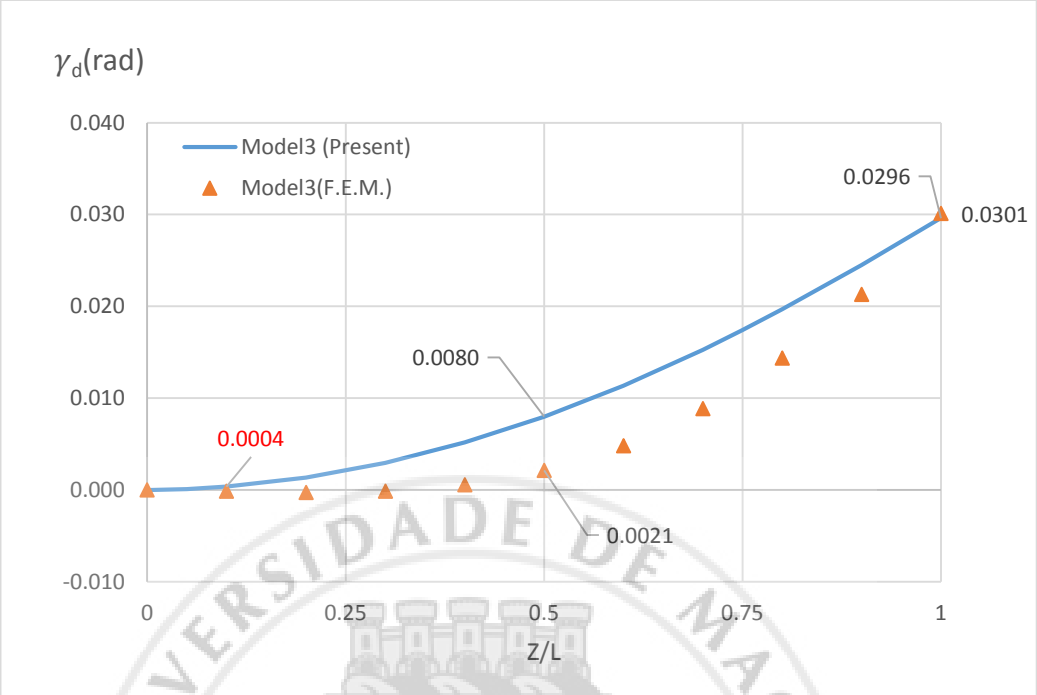

Fig. 5.3.3 - Distortional Angle distribution, (L = 1500mm, b=h=150mm)

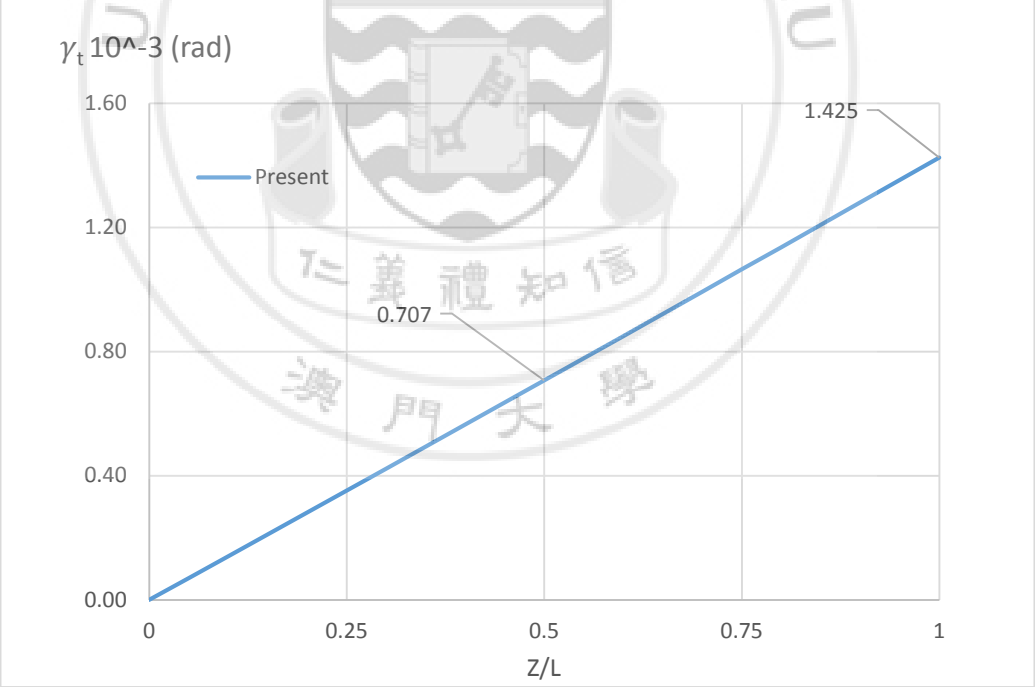

Fig. 5.3.4 - Twisting angle distribution, (L = 1500mm, b=h=150mm)

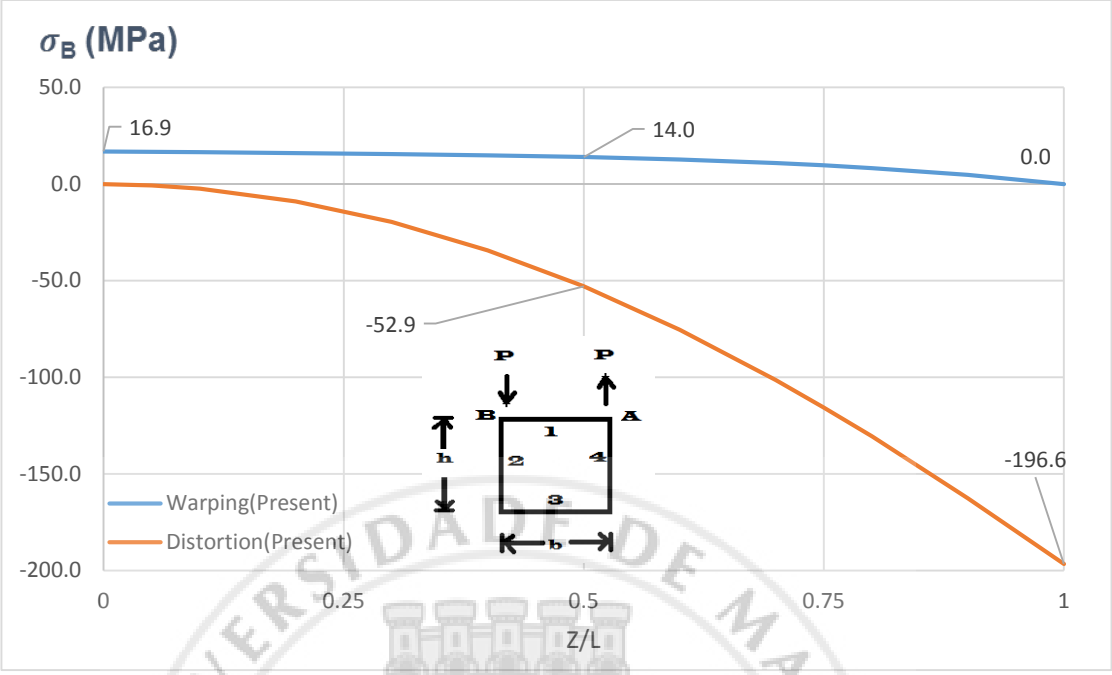

Fig. 5.3.5 - Distortion and warping stress distribution of corner B, (L = 1500mm, b=h=150mm)

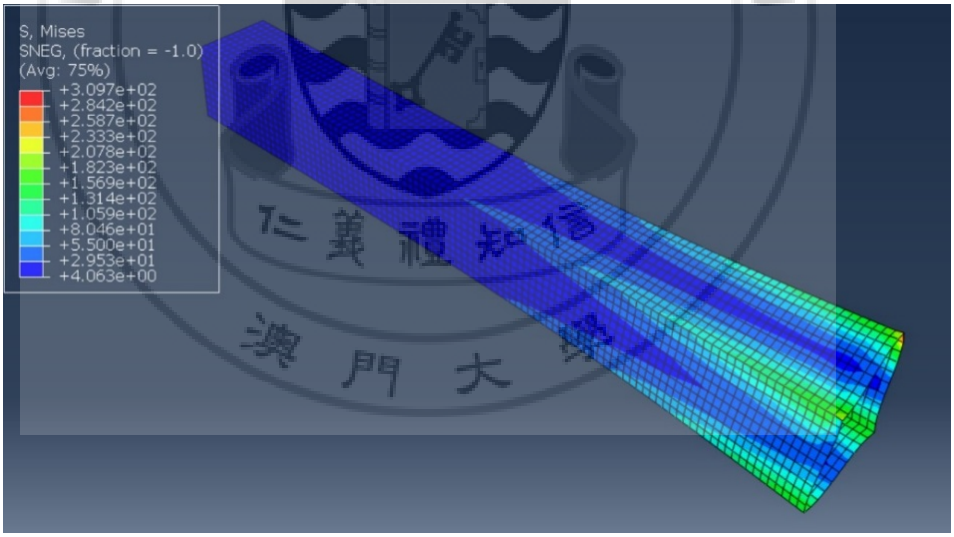

Fig. 5.3.6 - Stress(misses) of the beam

From Fig.5.3.5 and Fig.5.3.6, the distortion stress has an increasing-slope along the beam and a flatter slope at first but with approximately equal maximum value of

(-196.61MPa) compared to Model1 (-195.84MPa). On the other hand, the warping stress (max : 16.89MPa) along the beam is significantly smaller than Model1 (max: 59.52MPa), together with the overall 3-dimesional deformations.

5.4 Model4

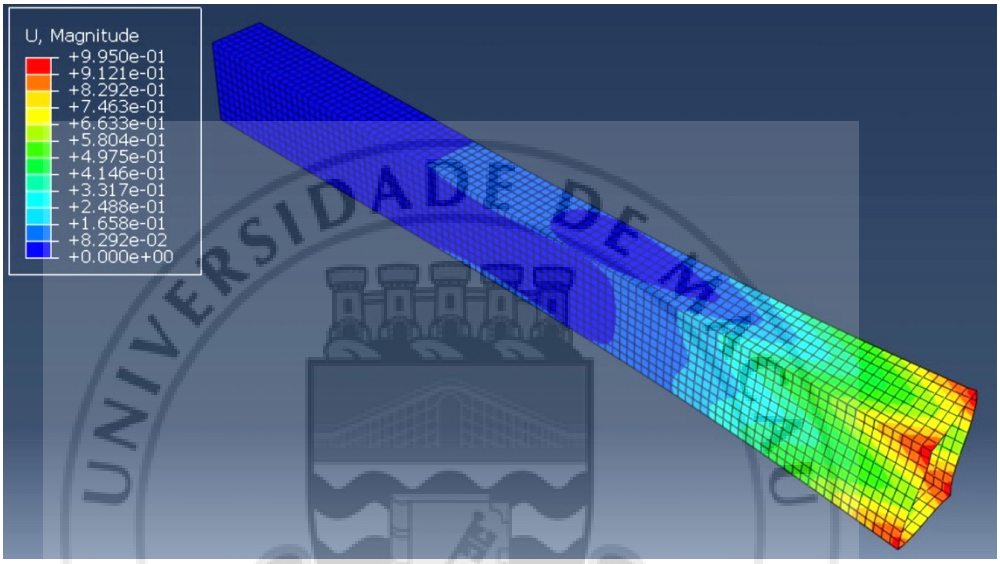

Fig. 5.4.1 - Deformed shape of the beam

Table 5.4 Relative error of 3-dimesional displacements

	u_s (mm)	u_n (mm)	u_z (mm)
Present Method	-0.718	1.005	-0.067
Abaqus	-0.713	0.684	-0.119
Relative Error	0.696%	31.9%	43.6%

To further analyze the effect on the deformation of the beam with different flange-width ratio, a flange-width ratio equals to 1:2 is used for Model4. From Fig.5.4.2(a), the tangential displacement has a positive value near the support and then becomes negative progressing to the free end. The axial decay effect is more significant than a square section which the abaqus model show nearly zero horizontal and warping deformations at mid-

span in Fig.5.4.2(b). Furthermore, the overall displacements of the cross-section are smaller with lower flange-width ratio, observations can be made that when using a wider flange with fixed web heights, more distorted cross-section and larger displacements are expected under same torsional loading. Note that the changing sense of u_s in Fig.5.4.2(a) and Fig.5.4.2(b) indicates that the cross-section does have a uniform distorted shape along the longitudinal axis. Fig5.4.3 shows that the top flange translates from right to left for a positive u_s value and the beam sway back to the right at the free end (Fig.5.4.4). A significant error occurred when analyzing lower flange-web ratio models due to the axial decay effect.

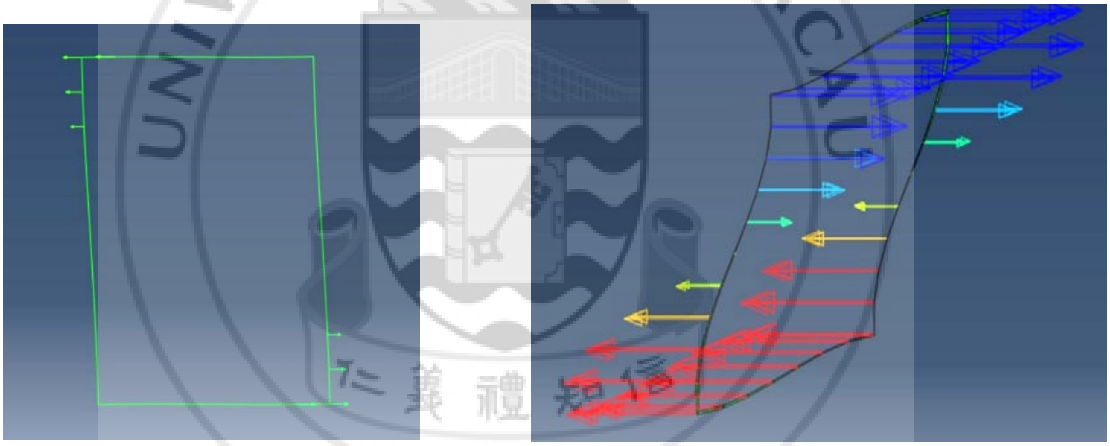

Fig. 5.4.3 Horizontal displacements at 3L/10 Fig. 5.4.4 Distorted shape at the free end

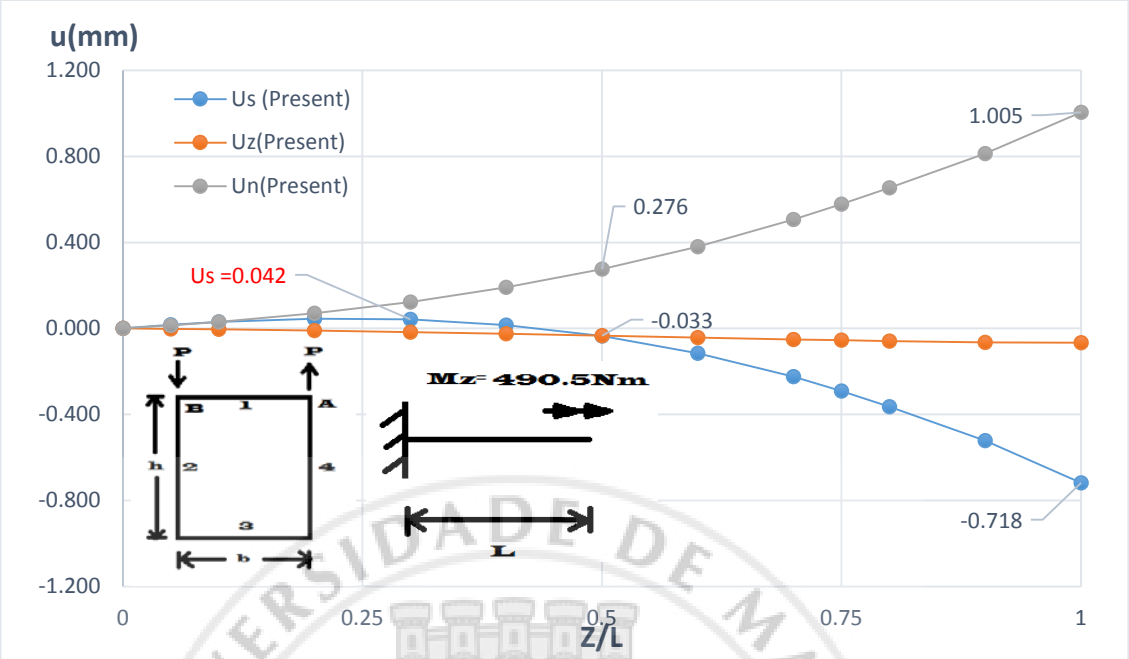

Fig. 5.4.2(a) 3-dimensional displacements of corner A (Present Method),(L = 1500mm, b = 100mm, h = 150mm)

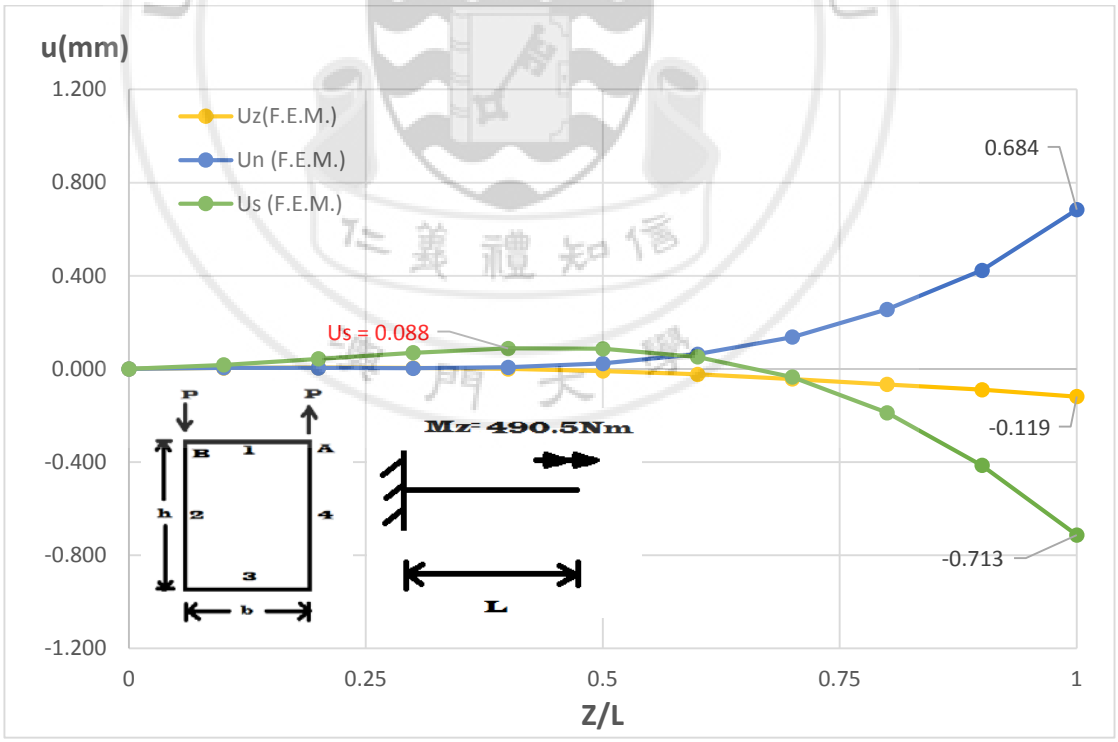

Fig. 5.4.2(b) 3-dimensional displacements of corner A (ABAQUS),(L = 1500mm, b = 100mm, h = 150mm)

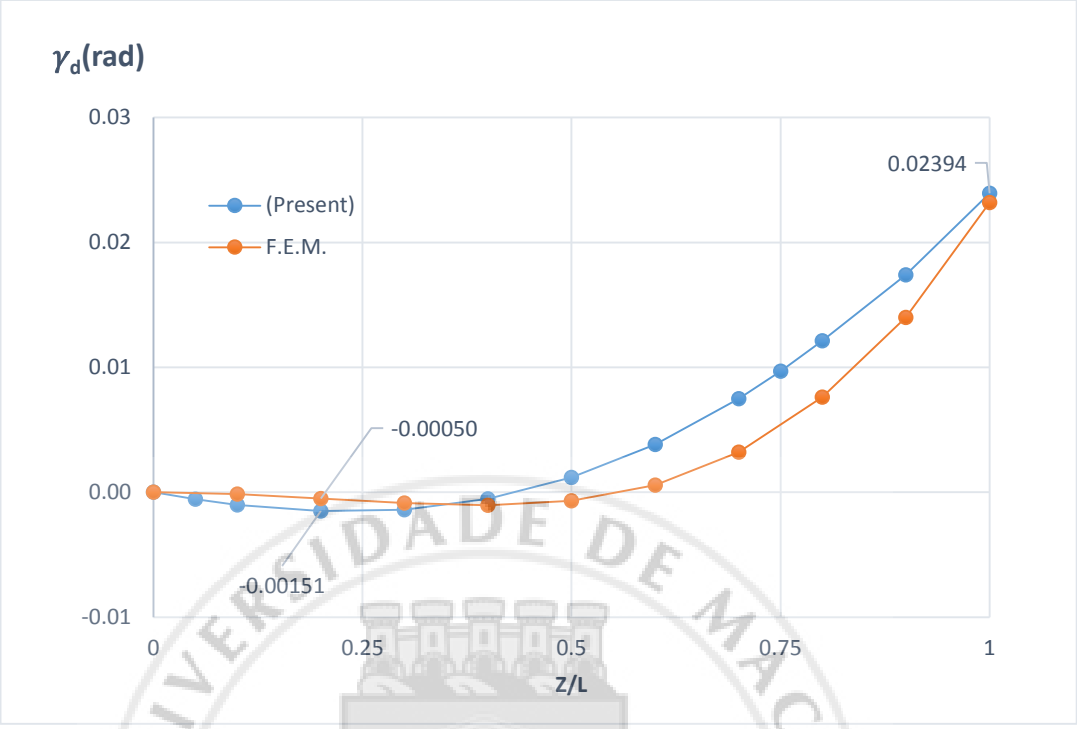

Fig. 5.4.3 - Distortional angle distribution along z-axis

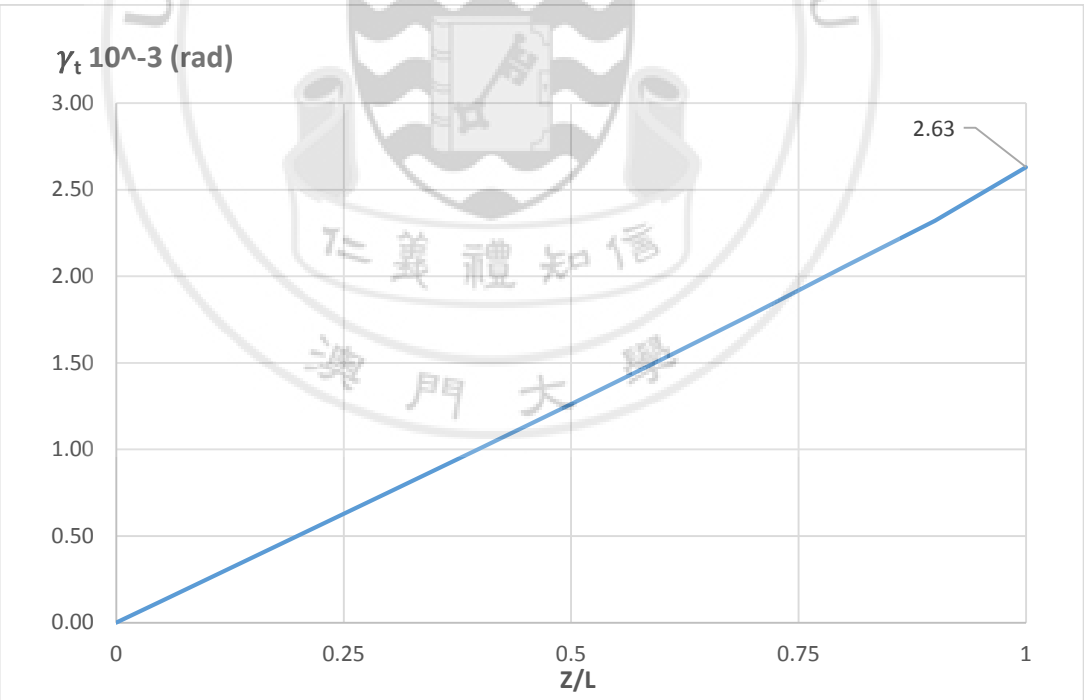

Fig. 5.4.4 - Twisting Angle distribution zlong z-axis

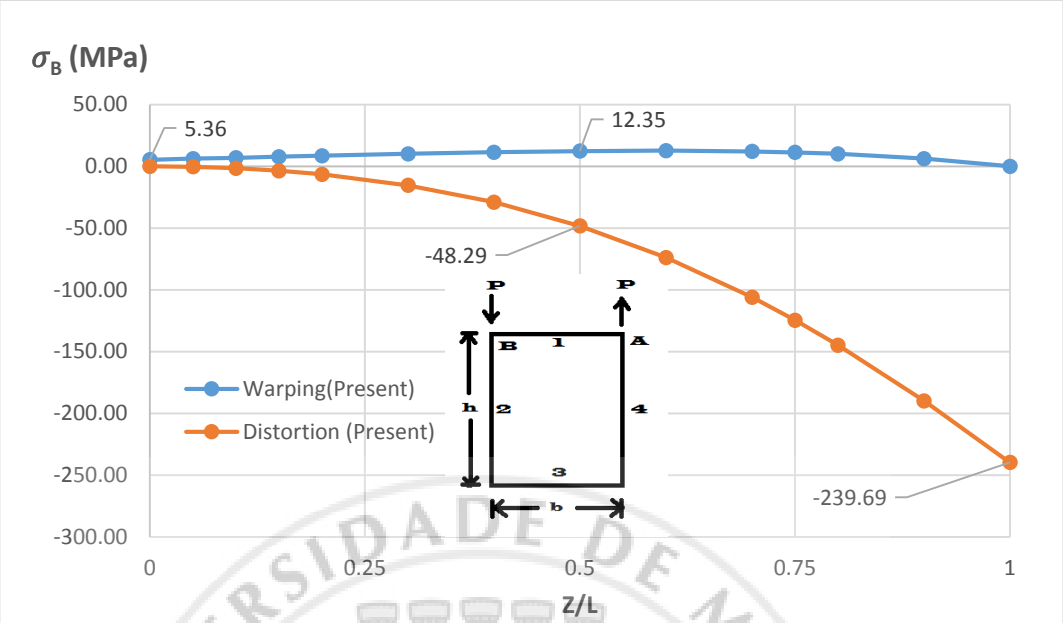

Fig. 5.4.5 - Distortion and warping stress of corner B

The distortional angle distribution along the beam is in fair agreement for the two results compared to Model3. The maximum warping does not occur at the fixed support (5.36MPa) but at the mid-span (12.35MPa). The Distortion stress has a maximum value at the free end (-239.69MPa) and zero at support. The major differences between Model1, Model3 and Model4 under same concentrated loading is that with a narrower flange the warping stress decreases but the distortion stress increases and a smaller overall deformation with the increasing axial decay effect.

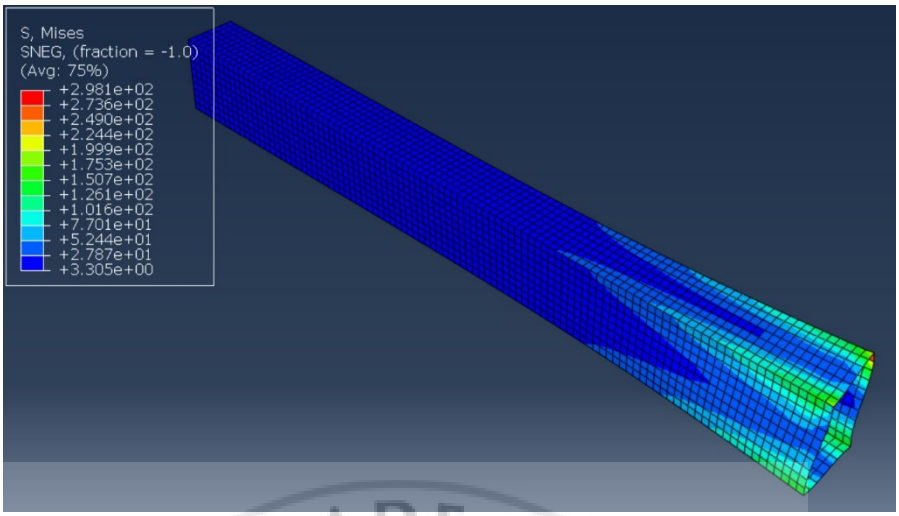

Fig 5.4.4 Stress (mises) of the beam

5.5 Model5

In model5, thicker walls (t = 6mm) are used, as shown in Fig.5.5.1, vertical and horizontal deformations are much smaller than using thickness = 3.18mm. The distortional angle (0.017rad) is also decreased more than half of the Model(0.045 rad)

Form Table.5.5.1 below, the overall deformation can be reduced more than half of Model1 when the thickness of the wall is doubled.

Table 5.5 Difference between Model1(t=3.18) and Model4(t=6)

Ratio = 6/3.48=1.89	u_s	u_n	u_z	γ_d	γ_t	σ_w	σ_d
Model1 (t=3.18mm)	-1.488	3.643	-0.221	0.045	0.00111	50	-195.84
Model5 (t=6mm)	-0.526	1.431	-0.089	0.017	0.00063	21.65	-140.13
% Decrease	64.6%	60.72%	59.7%	62.2%	43.2%	56.7%	28.4%

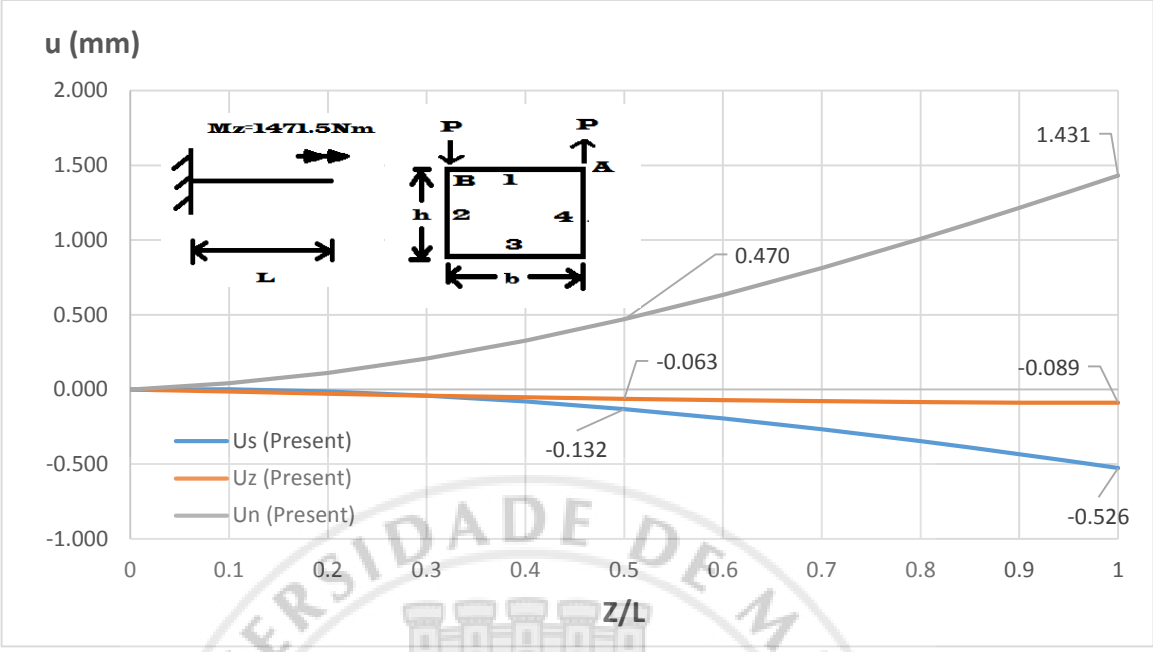

Fig. 5.5.2 – 3-dimensional displacements of cornerA

(L=1500mm,b=300mm,h=150mm,t=6mm)

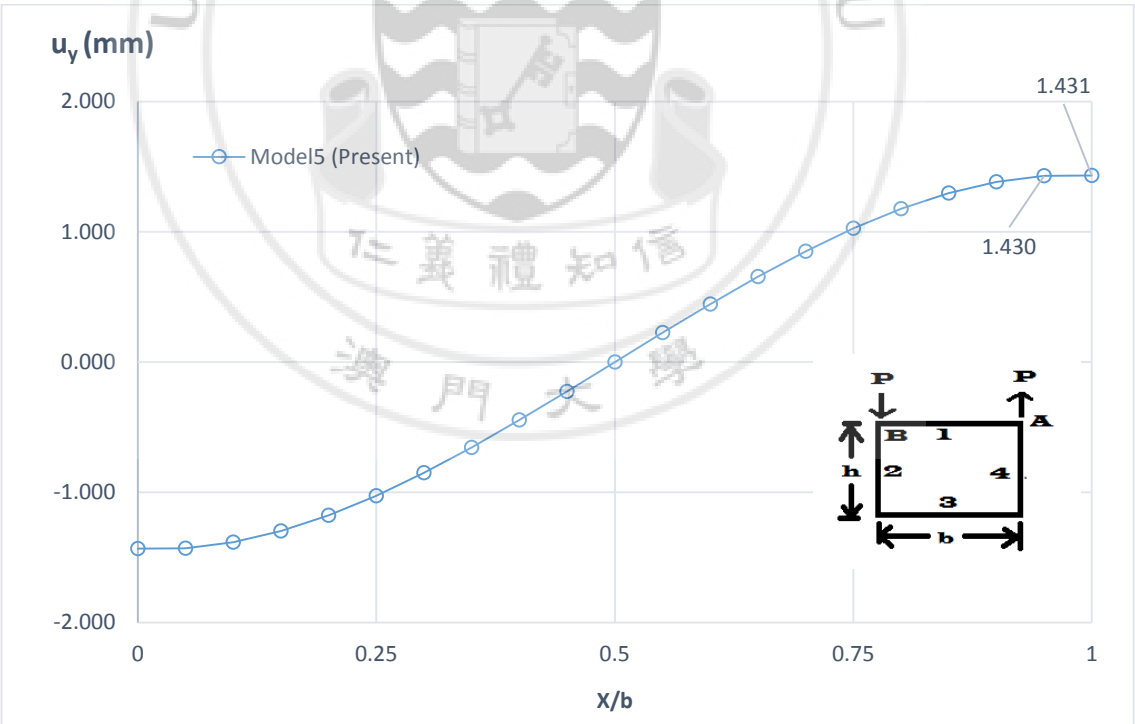

Fig. 5.5.3 Vertical Displacement(Un) distribution along top flange(wall1) at z = L

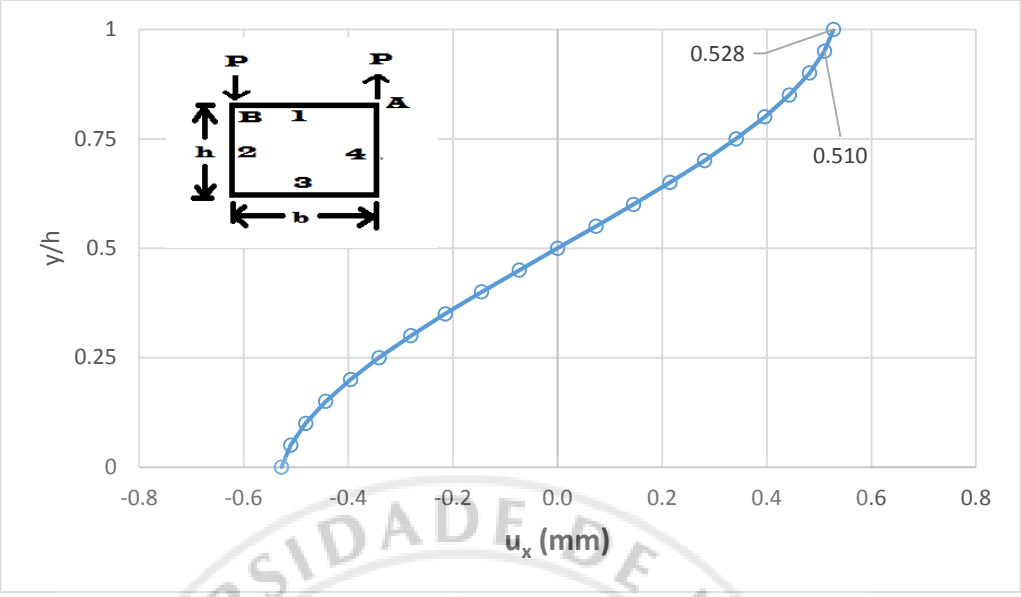

Fig. 5.5.4 Horizontal displacement(Un) distribution along right web(wall4) at z = L

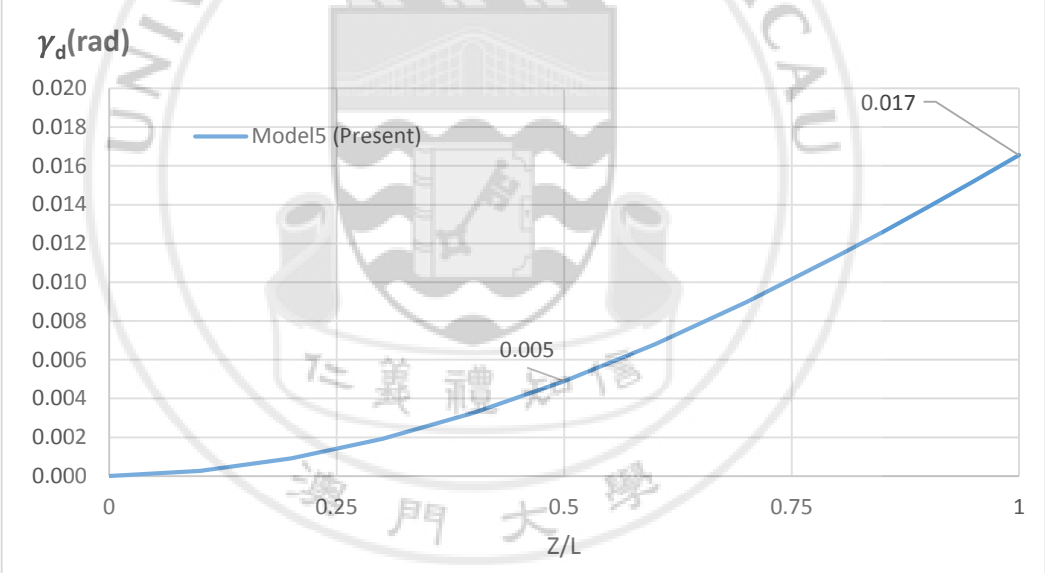

Fig. 5.5.6 Distortional angle along z-axis, L= 1500mm

The distortional angle and twisting angle (0.017,0.00633 rad)obtained are proportionally less than Model1 which has a thickness = 3.18mm (0.045,0.00111 rad). Also, the distortional and warping stresses can also be reduced for the box beam design if a thicker wall is used. However for the thin-walled analysis, for t greater than 1/10 of the wall length, the theoratical solutions may cause a significant error.

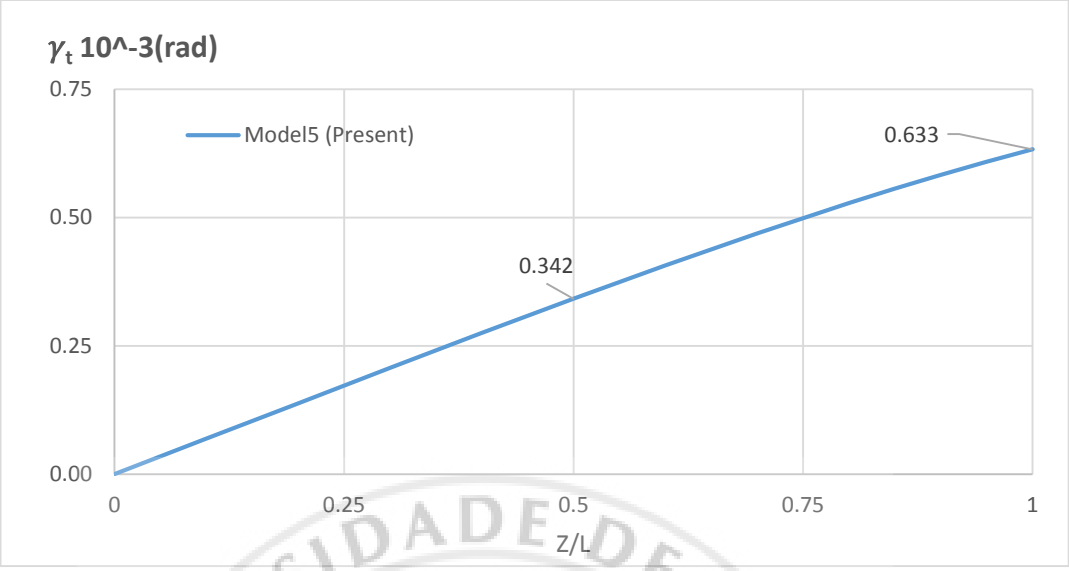

Fig. 5.5.7 Twisting angle along z-axis, L = 1500mm

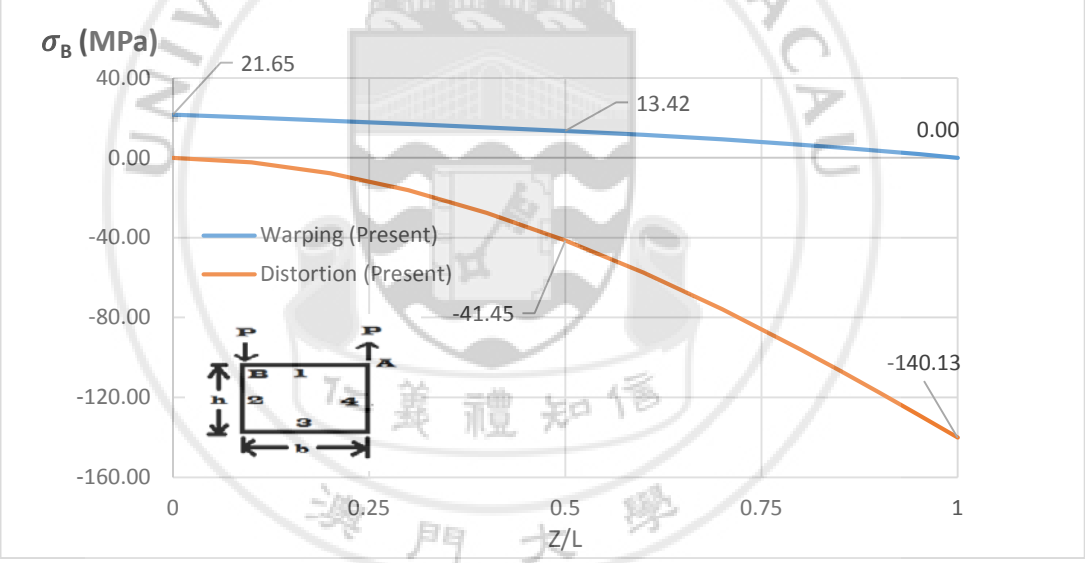

Fig. 5.5.8 The Distortion and warping stress distribution of corner B, L = 1500mm

Fig.5.5.8 shows the distortion and warping distribution along beam, the maximum stresses can be reduced under the same loading by increasing the thickness of the walls. Although the deformations can be reduced using a narrower flange but ideally a wider flange is desired as larger loading area can be provided. As an alternative the stresses can be reduced with a thicker contour to obtain smaller deformations.

5.6 Model6

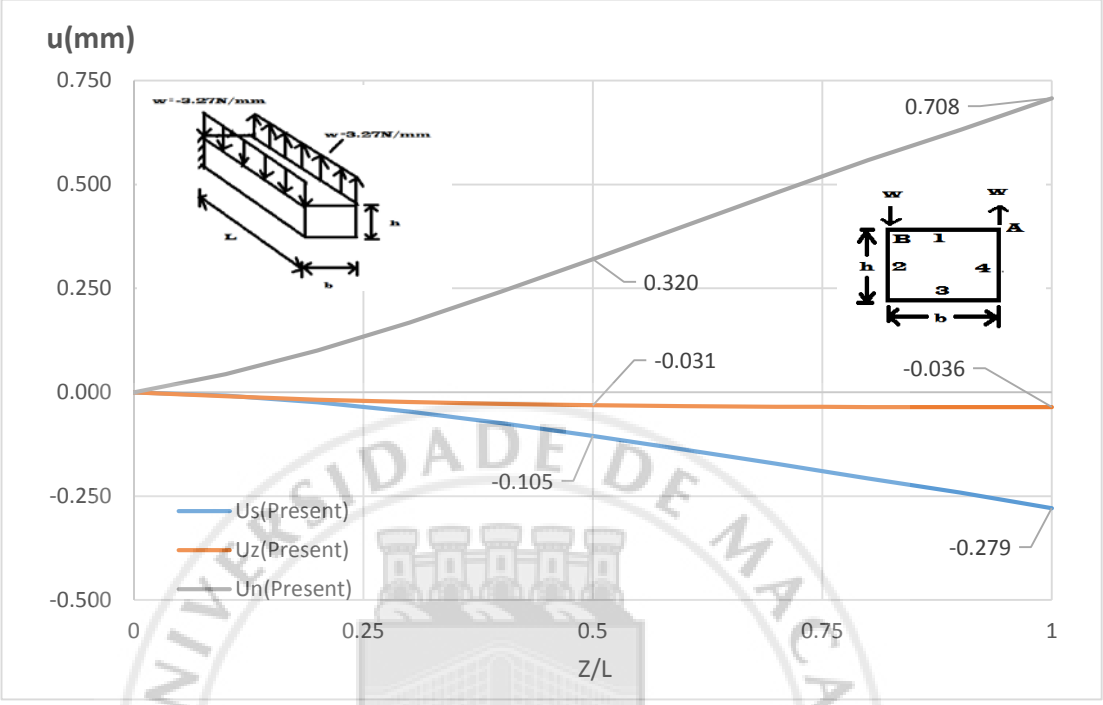

Fig. 5.6.1 3-Dimensional Displacements of corner A

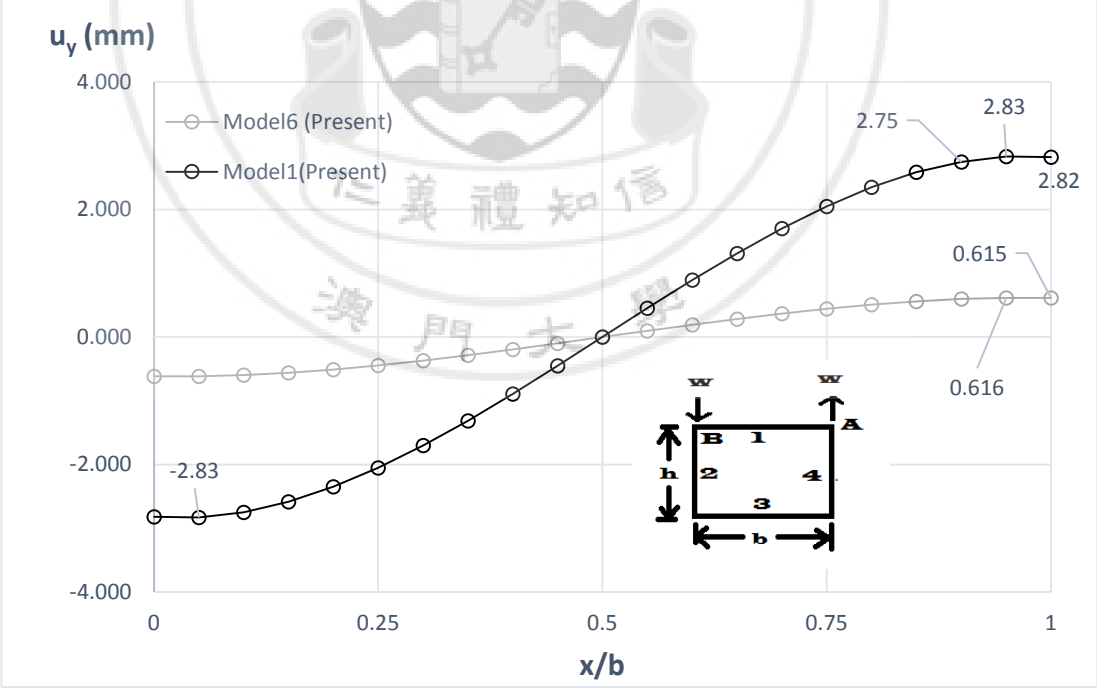

Fig. 5.6.2 Vertical displacement at 7/8span of Model1 and Model6

From Fig.5.6.1, the slopes of the change of the 3-dimensional deformations reflect a linear increase along the beam but a similar trend with Model1. The vertical displacement distribution along top flange at $7l/8$ is also compared to Model1, though, the vertical (Fig.5.6.2) and horizontal displacements (Fig.5.6.3.) changes more linearly than Model1, so as the horizontal displacements.

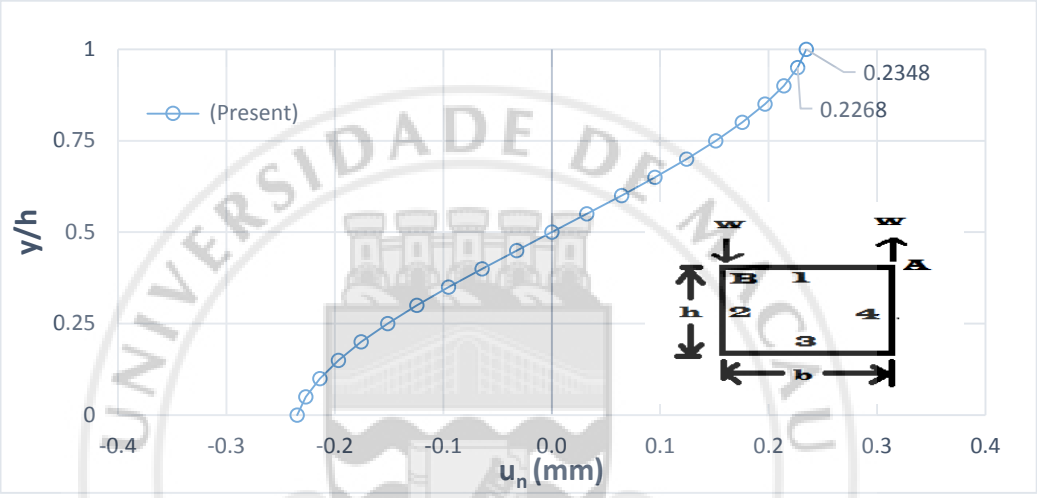

Fig. 5.6.3 Horizontal displacement distribution along right web(wall1) at free end

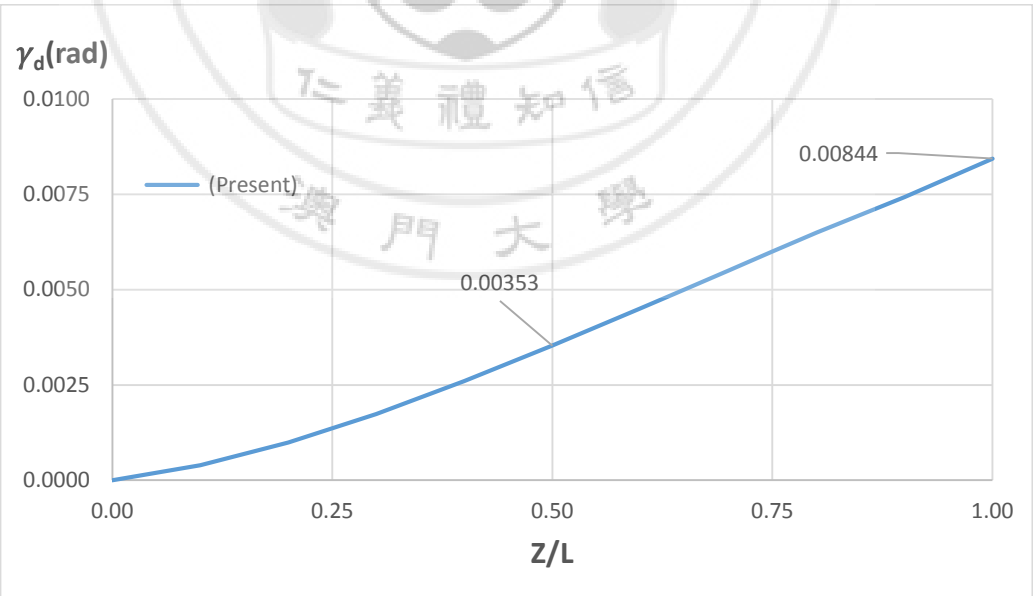

Fig. 5.6.4 Distortional angle distribution along z-axis

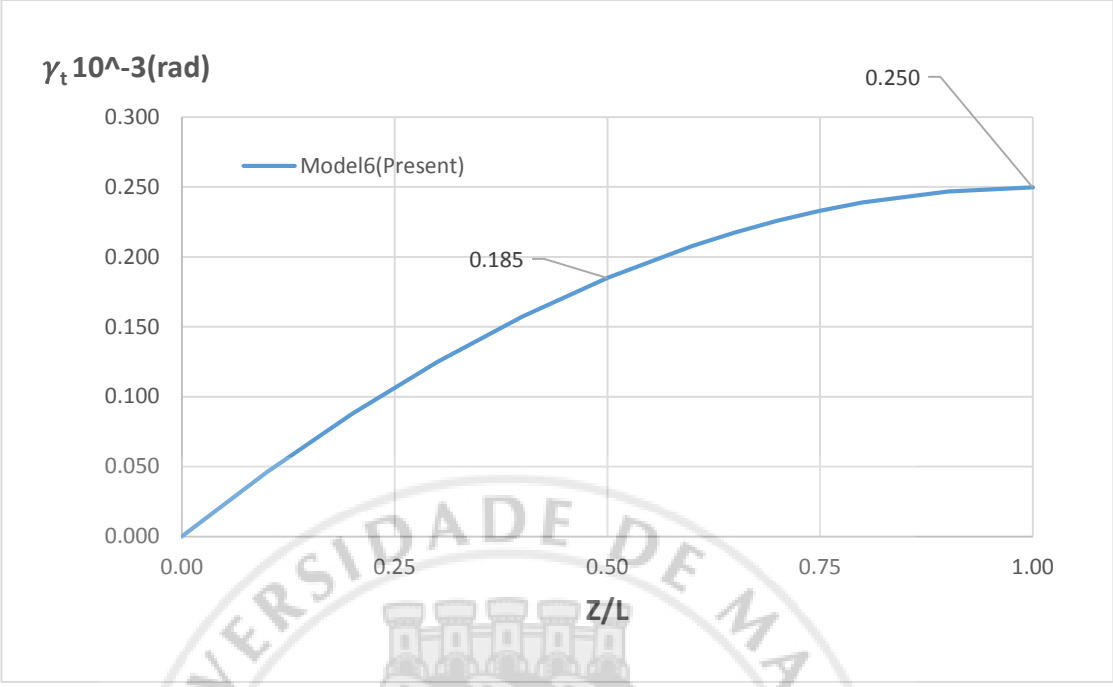

Fig. 5.6.5 Twisting angle distribution

The distortional angle increases linearly and has a maximum value of 0.00844 rad(Fig.5.6.5). The distributed load has equivalent vertical loading as Model1. The Twisting angle is a concave-down curve as it is increasing slower and slower towards the free end. Considering the stresses, the warping stress is now a concave-up curve rather than concave-down from the previous models while the distortion stress shows a similar change as Model1. For practical situations, loading on a box girder does not always concentrate on the free end and the girder is not likely to be a cantilever. However, the torsional loading has a similar effect with vertical loadings on a beam under comparison with concentrated and distributed loadings.

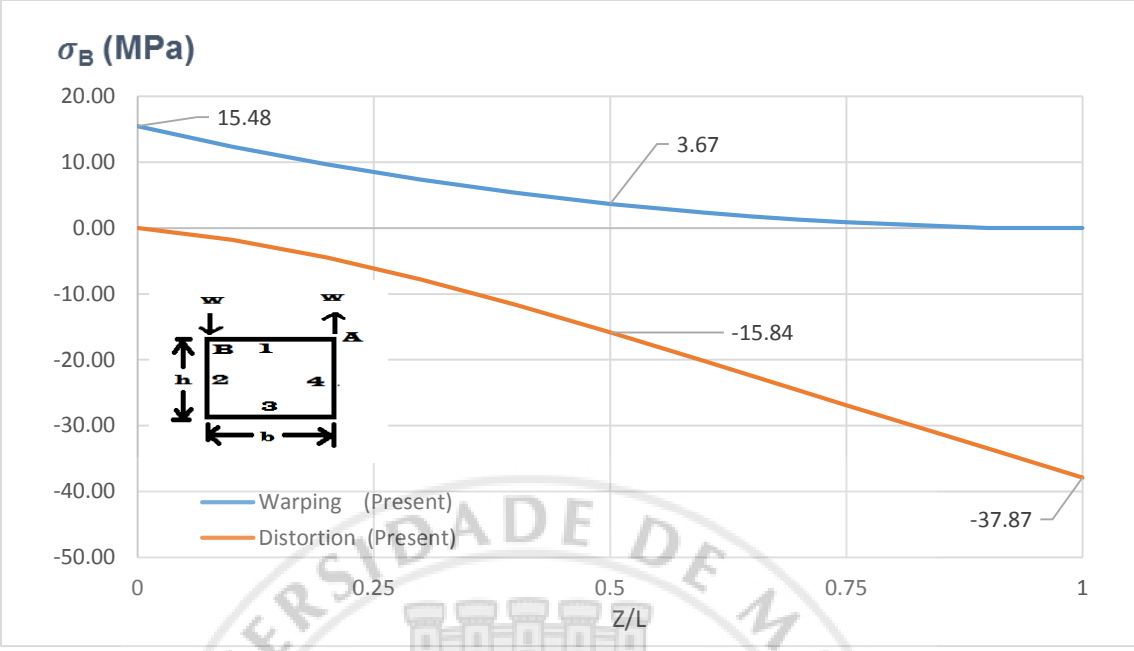

Fig. 5.6.6 Distortion and warping stress distribution of corner B

Conclusion and Suggestion

The torsional warping and distortion deformation of thin-walled box beams under torsional loading had been studied in the project. The tangential, normal and warping displacements of the contours can be estimated using the one-dimensional finite element theory by selecting appropriate pre-assigned functions. Under concentrated or distributed torsional loading, the warping displacement is relatively smaller than the distortional displacements and significant errors occurred when calculating the warping deformations which may due to error in computer programming. For general design approach, a lower flange-web ratio gives smaller warping stress but a larger distortional stress compared to a higher flange-web ratio section.

The distortional deformation of flange-web ratio lower than or equals to one were also predicted differently with those have higher flange-web ratio. The distortional angle varies along the beam with changing senses for certain cases. The continuity condition of the rotation of corners and the pre-assigned function could be used to predict the general warping and distortion deformation of thin-walled box beams. Furthermore, the result shown that thin-walled box beams have a high torsional rigidity as the twisting deformation is relatively small compared to the distortional deformation.

In future study, effort could be made on studying curved thin-walled girders under unsymmetrical loadings and the accuracy of the thin-walled theory with varying thickness could be verified.

References

- Balch, C.D. and Steele, C.R., 1987, "Asymptotic Solutions for Warping and Distortion of Thin-walled Box Beams", ASME Journal of Applied Mechanics, Vol.54, pp. 165-173.
- Boswell,L.F., and Zhang,S.H., 1983, "A Box Beam Finite Element for the Elastic Analysis of Thin-Walled Structures", Thin-Walled Structures, Vol.1 pp.353-383.
- Boswell,L.F., and Zhang,S.H., 1985, "An experimental Investigation of the Behavior of Thin-walled Box Beams", Thin-Walled Structures, Vol.3 pp.35-65.
- J.H. Kim, Y.Y. Kim, ,1999 , "Analysis of Thin-walled Closed Beams with General Quadrilateral Cross-Sections", ASME, p.904-p.915/Vol. 66
- Vlasov, V.Z., 1961, Thin-walled Elastic Beams, Isarel Program for Scientific Translations, Jerusalem.
- Wright, R. N., Abdel-Samad,S.R., and Robinson, A.R., 1968, "BEF" Analogy for Analysis of Box Girders," *J.Struct. Div*., ASCE, Vol.94, (ST7), pp.1719-43